Heat transfer enhancement in suspensions of agitated solids. Part III: Thermophoretic transport of nanoparticles in the diffusion limit.

Michel Louge[a]* and Xinglong Chen[a]

[a]Sibley School of Mechanical and Aerospace Engineering, Cornell University, Ithaca, NY 14853, USA

We illustrate the diffusion limit of wall heat transfer in fluid-solid suspensions by considering small colloidal particles dilute in a liquid at rest. Because such particles are agitated by Brownian motion, their self-diffusivity is modest, the fluid and solid phases share the same temperature, and mixture theory should predict the effective suspension conductivity. We show how thermophoresis creates suspension inhomogeneities, suggest ways to mitigate the latter with ultrasonic forcing, and examine consequences on heat transfer. To inform a debate on nanofluids heat transfer, we show that anomalous conductivity enhancements reported with hot-wire thermal conductimetry can be an experimental artifact of thermophoretic migration along the temperature gradient or timing in the observations.

keywords: nanofluid heat transfer, thermophoresis, ultrasound, resuspension, hot-wire conductimetry, diffusion limit

1. Introduction

In Part I of this paper, we outlined a theory for the enhancement of heat transfer at the wall of a vessel containing agitated spherical grains suspended in a conductive fluid [1]. We distinguished two asymptotic regimes, which we called the "exchange" and "diffusion" limits. In the first, heat transfer is set by the volumetric heat exchange rate between the two phases, and it may be further enhanced by particle-fluctuation-induced fluid thermal diffusion. In Part II, we tested the theory in that limit with relatively dense suspensions of millimetric spheres vigorously shaken in a box, through which heat was transferred between a cold and a hot wall. Part III now illustrates the diffusion limit by considering small "nanoparticles" dilute in a liquid at rest.

With few exceptions, dilute nanoparticle suspensions exhibit higher effective conductivities $k_{\rm eff}$ than the base fluid k_g [2,3], and $k_{\rm eff}/k_g$ grows linearly with the average solid volume fraction $\bar\nu$. Although many such observations can be explained by homogenization models inspired by Maxwell's [4,5], there are cases, mostly associated with small metal particles at low $\bar\nu$, for which the heat transfer enhancement exceeds these predictions [6]. Several mechanisms have been considered, including ballistic phonons within grains [7], Brownian diffusion [8] and enhanced Brownian diffusion [9,10], clustering [7,11,12] and highly anisotropic clustering [13], interfacial resistance through layering of liquid molecules [7,14–16], near-field interactions [17], hyperbolic heat conduction [18] and thermophoresis [19].

The objective of Part III is to outline the peculiar heat transfer mechanisms that occur in the diffusion limit with small particles. To that end, we derive and discuss governing equations for fluid-solid suspensions at rest subject to thermophoresis, particle resuspension and ultrasonic forcing. Because thermophoresis creates time-dependent inhomogeneities in the suspension, and because anomalously high $k_{\rm eff}$ have arisen with hot-wire thermal conductimetry [6], while spectroscopic techniques have not reported such enhancements [20,21], we also examine the performance of hot-wires in an attempt to inform a current debate on the subject. We begin by

*Corresponding author. Voice (607) 255 4193; fax (607) 255 1222; electronic mail: Michel.Louge@cornell.edu.

Table 1
Nomenclature

A_{132}	Hamaker constant
B, C	constants in Eqs. (19)
c_g, c_s	fluid, solid specific heats per mass
c_w, c_p	wire, sheath specific heats per mass
C_d	drag coefficient
d	grain diameter
D_s, D_T	particle, Soret self-diffusivities
$D_{\text{s-e}}$	Stokes-Einstein diffusivity
D_u, D_ν	ultrasonic, settling diffusivities
$\mathbf{e}_y$, $\mathbf{e}_r$	wall normal, wire radial unit vectors
f	ultrasonic frequency
$\mathbf{F}$, $\mathbf{F}_u$, $\mathbf{F}_v$	net, ultrasonic, van der Waals forces
g_{12}	binary sphere pair distribution
h_g, h_s	fluid, solid sensible mass enthalpies
$\imath$	$\imath^2 = -1$
I	ultrasonic energy flux
$\mathbf{j}_g''$, $\mathbf{j}_s''$, $\mathbf{J}''$	fluid, particle, resuspension fluxes
k_b	Boltzmann's constant
k_g, k_s, k_a	fluid, solid, apparent conductivities
k_{cl}, k_{eff}	cluster, effective conductivities
k_p, k_w	sheath, wire thermal conductivities
K_g, K_s, $\bar{K}$	mixture, solid, channel conductivities
L	wall-to-wall distance, vessel size
$L^\dagger$	relative length scale in Eq. (2)
ℓ, ℓ_s	grain diffusion, Stokes lengths
m	grain mass
$M^\dagger$	excess or deficit of mass in Eq. (68)
n_ℓ	number of adhered particle layers
$\mathbf{n}$	ultrasonic wave direction
N, N_0	surface particle number densities
$\mathbf{q}$, $\mathbf{q}_g$, $\mathbf{q}_s$	Fourier fluxes in mixture, fluid, solid
q^+, q^-	heat fluxes at hot, cold walls
$\dot{q}$	heat rate supplied per wire length
r	radial coordinate
r_w, r_p	wire core, sheath outer radii
$R^\dagger$	relative domain size around the wire
R_d	hindered settling function in Eq. (34)
S	ultrasound speed
t, t_f	time, period to solve Eqs. (61) & (62)
T, T_g, T_s, T_w	mixture, fluid, solid, wire temps.
T_m	mixed-mean-temperature in Eq. (43)
T_∞, T^+, T^-	ambient, cold, hot wall temperatures
$\mathbf{u}$, $\mathbf{v}$	fluid, particle velocities
v, v_b	grain, Brownian diffusion speeds
$\mathbf{v}_T$, $\mathbf{v}_u$, $\mathbf{v}_t$	thermophoretic, ultrasonic, settling vels.
v_i'	grain fluctuation velocity along i
y	cartesian coordinate

Table 2
Greek

α	suspension thermal diffusivity
α_p, α_w	hot-wire sheath, wire thermal diffusivities
α_1, β_1	functions in Eq. (23)
β	thermophoretic coefficient
γ	Euler's constant
η_0, η	adhesion gaps
Θ	granular temperature
ι	variable of integration
λ_s	grain mean free path
μ_1, μ_2, μ_3, μ_4	functions in Eq. (23)
μ	fluid viscosity
ν	solid volume fraction
ν_a	fraction of volume occupied by clusters
ν_{cl}	solid volume fraction within a cluster
ν_c	randomly jammed solid volume fraction
ν_s	surface fraction of adhered particles
ξ_s	k_s/k_g
ρ_g, ρ_s, ρ_w, ρ_p	fluid, solid, wire, sheath material densities
$\overline{\rho c}$	mean volumetric specific heat
τ_s, τ	viscous, adhesion relaxation times
ω	relative ultrasonic particle size in Eq. (22)
ω_v	relative ultrasonic viscous length in Eq. (22)

Table 3
Dimensionless groups

$C^\dagger$	$(\rho_g c_g)/(\rho_s c_s)$
Da	Damköhler second ratio
Kn	Knudsen number
Le, Le∞	Brownian Lewis numbers
Nu	particle Nusselt number
Pe_s	ultrasonic Péclet number
Pr	Prandtl number
St	particle Stokes number
Γ_r	dimensionless resuspension number
$\bar{\theta}$, θ_∞	dimensionless temperatures
Π	$2(\overline{\rho c})/(\rho_w c_w)$

Table 4
Scripts

†	dimensionless
–	spatial average
+/−	hot/cold walls
<>	velocity distribution average
crit	critical value
g, s	fluid, solid
p, w	sheath, wire core

contrasting mechanisms of heat transfer in the exchange and diffusion limits.

2. Diffusion-limited conduction in uniform suspensions at small temperature gradient

In this section, we contrast mechanisms of self-diffusive heat transfer for large and small particles in a suspension with no average velocity, uniform solid volume fraction and vanishing thermal temperature gradient. In Part I, we showed that particle velocity fluctuations play a role in enhancing the effective suspension thermal conductivity. Because particles seldom have enough time to exchange heat directly with solid surfaces, the enhancement of heat transfer that they create is a competition between two rate-limiting processes, namely their ability to self-diffuse through the suspension, and to exchange heat with the surrounding fluid. These processes are arbitrated by a Damköhler second ratio

$$\mathrm{Da} \equiv \frac{(K_g/K_s)(L^\dagger/2)}{\tanh(L^\dagger/2)}, \tag{1}$$

with dimensionless length scale

$$L^\dagger \equiv \frac{L}{d}\sqrt{12\nu\mathrm{Nu}\Big(\frac{k_g}{K_g}+\frac{k_g}{K_s}\Big)}. \tag{2}$$

In these expressions, K_g is the mixture conductivity, which, at low values of the local solid volume fraction ν, is well captured by Maxwell's model in terms of the ratio $\xi_s \equiv k_s/k_g$ of the respective material conductivities k_g and k_s of the pure fluid and solid [22],

$$\frac{K_g}{k_g} = \frac{(2+\xi_s)+2\nu(\xi_s-1)}{(2+\xi_s)-\nu(\xi_s-1)}; \tag{3}$$

K_s is the conductivity of the agitated solid phase arising from particle self-diffusion; L/d is the ratio of vessel size and particle diameter; and Nu is the Nusselt number characterizing the heat exchange between a particle and the surrounding fluid. The rate-limiting processes give rise to two asymptotic regimes.

In the first regime ($\mathrm{Da} \to 0$), which we call the "exchange limit", solids agitation is so intense that the thermal temperatures of fluid and solids are significantly different. In fact, it is the difference between these two temperatures that determines the enhancement of k_{eff} through the volumetric rate of heat transfer that couples the solid and fluid phases. In that limit, the magnitude of particle agitation is too large to matter, unless it induces velocity fluctuations in the fluid, thereby raising k_{eff} further through a mechanism similar to turbulence. In Part II, we tested the theory in the exchange limit by conducting experiments with millimetric spheres shaken in a box, for which k_{eff}/k_g rose up to ~ 20.

The other asymptotic regime is where particle agitation is more modest and/or length scales are large ($\mathrm{Da} \to \infty$). In this "diffusion limit," the thermal temperature T_g of the fluid and its counterpart T_s for the dispersed solid phase are equal, $T = T_g = T_s$, and, as we showed in Part I, the effective conductivity is merely the sum of the mixture conductivity and a contribution arising from the self-diffusion of solids,

$$k_{\mathrm{eff}} = K_g + K_s. \tag{4}$$

In fluid-particle systems with vanishing average velocity, agitated particles self-diffuse through the suspension even without a concentration gradient. This gives rise to a thermal conductivity of the solid phase

$$K_s = \rho_s \nu c_s D_s \ , \tag{5}$$

where ρ_s and c_s are, respectively, the material density and specific heat per mass of the solids.

Because the temperatures of the two phases are identical, the rate of heat exchange between the phases is negligible, and thus the strength of that exchange does not matter to the effective conductivity. In particular, the magnitude of the Nusselt number in Eq. (2) is irrelevant to $k_{\rm eff}$.

Because of their relatively small size ($L/d \ll 1$) and modest agitation, colloidal "nanoparticles" belong to the diffusion limit. Together with the surrounding fluid, they form a mixture at a single thermal temperature with an effective conductivity $> K_g$. In the two sub-sections that follow, we contrast their ability to produce a significant K_s with that of macroscopic, massive particles.

2.1. Massive particles

In Parts I and II, we considered "massive" grains characterized by a high Stokes number ${\rm St} \equiv \tau_s\sqrt{\Theta}/d \ggg 1$, where $\tau_s = m/(3\pi d\mu)$ is the particle viscous relaxation time, μ is the fluid viscosity, and m is the particle mass. Such massive grains are unaffected by fluid velocity fluctuations. Instead, their dynamics is dominated by inertia. In a dense "gas" composed of such granular hard spheres with fluctuation velocity v_i' in the cartesian direction i, agitation is measured with the "granular temperature" $\Theta \equiv (1/3)\overline{v_i'v_i'}$ that is analogous to the translational temperature introduced in the kinetic theory. Note that Θ bears no relation to the usual thermal temperature of the particles, which we denote with the distinct symbol T_s. For nearly elastic, massive granular solids, this agitation gives rise to a self-diffusion with coefficient

$$D_s = \frac{d\sqrt{\Theta}}{(9\sqrt{\pi})\nu g_{12}}\Big(\frac{1}{1+2{\rm Kn}}\Big), \qquad (6)$$

where $g_{12}(\nu)$ is the Carnahan and Starling pair distribution function [23]

$$g_{12} = \frac{2-\nu}{2(1-\nu)^3}, \qquad (7)$$

and the term in parentheses is a correction for high Knudsen number ${\rm Kn} = \lambda_s/L$ [24,25] that is significant when the granular mean free path $\lambda_s = d/[6\sqrt{2}\nu g_{12}]$ between consecutive impacts is on the order of the vessel size L. Thus, at large L/d and small ν, one recovers the classical scaling for the self-diffusion of a gas of hard spheres,

$$D_s \sim \ell v, \qquad (8)$$

where, in this case, the characteristic diffusion length is the mean free path $\ell \sim \lambda_s$ and the diffusion velocity $v \sim \sqrt{\Theta}$. The Knudsen correction in Eq. (6) guarantees that K_s vanishes as $\nu \to 0$ in vessels of a finite size. However, with small enough particles or large vessels, it is superfluous, ${\rm Kn} \sim 0$. For large enough L/d, and for small ν such that $g_{12} \sim 1$, Eqs. (5) and (6) predict that the thermal conductivity K_s of the granular phase is independent of ν, a fact related to Maxwell's 1860 paradox of a viscosity independent of pressure [25].

A consequence is that, for massive granular solids in the diffusion limit, agitation can enhance $k_{\rm eff}$ at very low volume fractions. In fact, upon combining Eqs. (3) to (7), the series expansion at vanishing ν

$$\frac{k_{\rm eff}}{k_g} = 1 + 3\nu\Big\{\Big(\frac{\xi_s-1}{2+\xi_s}\Big) + \sqrt{2}\Big(\frac{L}{d}\Big){\rm Pr}_s + o(L/d)^{1/2}\Big\} + o(\nu^2) \qquad (9)$$

reveals that, as massive agitated grains are first introduced in a fluid, $(k_{\rm eff}/k_g)$ rises rapidly with ν at a steep slope $\sim 3\sqrt{2}(L/d){\rm Pr}_s$ to the more gentle linear variation

$$\frac{k_{\rm eff}}{k_g} = 1 + 3\nu\Big(\frac{\xi_s-1}{2+\xi_s}\Big) + {\rm Pr}_s + o(\nu^2), \qquad (10)$$

in which the dependence on ν is solely attributed to K_g/k_g, as soon as ν exceeds the small critical value $1/(3\sqrt{2}L/d)$. In Eqs. (9) and (10), ${\rm Pr}_s \equiv d\sqrt{\Theta}/[9\sqrt{\pi}(k_g/\rho_s c_s)]$ resembles a Prandtl number. For particles of high material conductivity relative to the fluid's ($\xi_s \gg 1$), the slope of $k_{\rm eff}/k_g$ versus ν is 3.

2.2. Dilute colloidal suspensions

The thermal diffusivity of small colloidal particles dilute in a viscous fluid has markedly distinct physics. The chief reason is that these particles are also subject to forces exerted on their surface, such as Stokes drag or Brownian impact, in addition to volume forces, such as inertia. They are

also subject to thermophoresis, whereby a temperature gradient ∇T induces particle migration and hydrodynamic diffusion, thus coupling particle motion to the temperature field. In this section, we restrict attention to temperature gradients that are too small to create significant thermophoresis. We revisit this assumption in the next section.

One important difference between massive grain and particles of low Stokes numbers is that the latter's diffusion length in Eq. (8) no longer depends on ν. Instead, this length is now the Stokes viscous relaxation distance

$$\ell_s \equiv \tau_s < \mathbf{v}_b^2 >^{1/2} \tag{11}$$

to a sudden jolt of the particle velocity to the rms diffusion velocity $v_b \equiv < \mathbf{v}_b^2 >^{1/2}$, where $<>$ denotes averaging over the velocity distribution, and v_b is the instantaneous fluctuation velocity of the Brownian particle in the fluid at rest. For such a particle of mass m at equilibrium with the surrounding liquid, $(m/2) < \mathbf{v}_b^2 >= (3/2)k_bT$, where $k_b = 1.38\ 10^{-23}$ J/°K is Boltzmann's constant. To within a constant of $o(1)$, the product $\ell_s v_b$ is the Stokes-Einstein diffusion [26]

$$D_{\text{s-e}} = \frac{k_bT}{3\pi\mu d}, \tag{12}$$

which is substituted for D_s in Eq. (5) to predict the corresponding conductivity of the particle phase. By analogy with Eq. (6), Cohen and de Schepper [27] proposed a simple heuristic correction of Eq (12) for arbitrary volume fractions, $D_{\text{s-e}} = (k_bT)/[3\pi\mu d g_{12}(\nu)]$, capturing reductions in $D_{\text{s-e}}$ at high ν associated with "cage" diffusion. Because $D_{\text{s-e}}$ is nearly independent of ν when the suspension is dilute, $K_s \propto \nu$. In the limit where $\nabla T \to 0$, the conductivity of the dilute particle phase is

$$\lim_{\nabla T \to 0} \left(\frac{K_s}{k_g}\right) = \frac{\rho_s c_s}{k_g}\ \frac{k_bT}{3\pi d\mu}\ \nu. \tag{13}$$

Consequently, with $\nabla T \to 0$ and $\nabla \nu = 0$, K_s is small at low ν, and it constitutes a negligible enhancement over the fluid conductivity: consider for example 6 nm copper nanoparticles suspended in ethylene glycol at $\sim$ 300°K, which have $k_{\text{eff}} > K_g$ [6]. For such suspension with $\rho_s = 8930$ kg/m^3, $c_s = 385$ J/kg°K, $k_s = 401$ J/m°K, liquid density $\rho_g = 1114$ kg/m^3, liquid specific heat per mass $c_g = 2415$ J/kg°K, $k_g = 0.252$ J/m°K, and $\mu = 0.0157$ kg/m.s, Eq. (13) predicts a ratio $K_s/k_g \sim 10^{-4}\ \nu \ll 1, \forall \nu$. In fact, Evans, et al [8] and Vladkov and Barrat [15] recently showed that the thermal diffusivity induced by Brownian motion is indeed negligible in most cases, and that it cannot explain the anomalous enhancement of k_{eff} observed with certain nanofluids [6]. Further, as we mentioned earlier, because k_{eff} is independent of Nu in the diffusion limit, nanoparticle suspensions cannot benefit from high particle-fluid heat exchange rates either [9,10,19,28].

Explanations for the observed enhancement of k_{eff} must be found elsewhere. Buongiorno [19] dismissed diffusiophoresis, Magnus forces, and settling under gravity. Free convection is also negligible at the small scale of typical devices unless transient measurements take too long [29]. Instead, Buongiorno suggested that thermophoretic transport may play a role at finite ∇T. However, because thermophoresis is driven by a temperature gradient largely determined by system geometry, its significance is not universal.

In this paper, we examine the role of thermophoresis for two systems. First, we analyze in the next section the semi-infinite channel with two parallel thermal walls considered in Part I. We derive governing equations for mass and energy and show that thermophoresis can induce significant particle migration. We suggest how the resulting inhomogeneities could be mitigated by applying ultrasonic forcing. Second, we consider the temperature field produced by hot-wire thermal conductimetry, which is employed in most nanofluids experiments. We assess the role of thermophoresis in clearing (or densifying) the region near the wire and in possibly resuspending particles previously adhered to it.

3. Particle migration at finite temperature gradient

A major difference between the heat transfer with macroscopic grains and small colloidal par-

ticles is that thermophoresis can gradually upset the distribution of solids in vessels where small particles are subject to a finite ∇T. To illustrate this, we now examine how thermophoretic inhomogeneities affect heat transfer in a generic channel similar to that of Part I. We also calculate whether ultrasounds could mitigate the formation of such inhomogeneities by opposing the thermophoretic force in a manner similar to ultrasonic particle separation [30,31].

3.1. Thermophoresis in liquids

In a dilute suspension, temperature gradients can drive a thermophoretic flux of particles. Upon interpreting their experiments with $\sim 1\mu$m latex spheres in water and n-hexane, McNab and Meisen [32] proposed a semi-empirical expression for the thermophoretic velocity by extending the gas-particle calculation of Epstein [33] to liquid-particle systems,

$$\mathbf{v}_T = -\beta \frac{\mu}{\rho_g} \frac{\nabla T}{T}, \tag{14}$$

for which they wrote

$$\beta \simeq 0.26 \Big(\frac{k_g}{2k_g + k_s} \Big) > 0 \ , \tag{15}$$

thus implying that such "positive" thermophoresis draws particles toward cold regions of the liquid. The coefficient in Eq. (15) is related to the Soret thermal diffusivity D_T using $\beta \equiv T D_T \rho_g / \mu$. Giddings, et al [34] warned that this fit of β, while suitable for neutral spheres, may seriously under-estimate the thermophoretic velocity of metal particles in a liquid. Effectively, they suggested that the value of k_s to substitute in Eq. (15) could be much smaller than the actual material conductivity of the metal particles depending on the form of their surface potential energy distribution.

To interpret her experiments on nanoparticles migration in a solvent using the beam deflection technique [35], Putnam [36] reviewed current theories and available data for thermophoresis in liquids. She noted that thermophoretic diffusion can be "negative" ($\beta < 0$) for aqueous suspensions of charged particles at low ionic strengths [37] and ferro-fluids [38], exhibit temperature dependence [39–41], and vary with volume fraction [40] and ionic concentrations [39]. As we will discuss in section 4, the possibility of negative thermophoresis, even with relatively low $|\beta|$, can have a profound influence on the apparent thermal conductivity recorded by hot-wire conductimetry.

Bringuier [42] recently warned that the concept of a thermophoretic velocity may be misleading, noting in particular how the temperature dependence of the thermophoretic mobility can reverse the sign of β. Nonetheless, Eq. (14) remains useful, so long as experimental data is interpreted in this framework [36,42]. In this paper, for simplicity, we take β to be invariant for each system. If instead, for example, temperature varies considerably, it would be relatively straightforward to capture more complex effects by letting β vary in the model [41]. We also ignore electrophoresis, which may be induced if electricity is the source of heat, and if particles have a high ζ-potential [36].

Because the thermophoretic and Stokes drag forces are both proportional to d, the thermophoretic terminal velocity in Eq. (14) has no explicit dependence on particle diameter. Consistent with this simple view, the data of Putnam and Cahill [36,39] and Vigolo, et al [43] suggest that β is independent of d. This does not mean that particles of any size would reach v_T. Macroscopic particles, for example, if subject to fluid inertia at a drag coefficient C_d, would reach $v_T \simeq 2\sqrt{6}[\mu/(\rho_g d)](\beta d/C_d)^{1/2} |\nabla \ln T|^{1/2} \propto 1/d^{1/2}$, and would generally experience negligible thermophoresis.

As long as suspensions remain dilute, we need not account for the dependence of v_T in Eq. (14) on solid volume fraction. However, if intense thermophoretic migration produces regions of high ν, then a first approximation to generalize Eq. (14) might be to substitute the mixture viscosity $\mu \exp(4.58\nu)$ provided by Happel and Brenner [44] for μ. Ning, et al [40] provide recent experimental insight on the role of ν.

3.2. Ultrasonic forcing

Following the works of King [45] and Yosioka and Kawasima [46] for the acoustic forcing of rigid and compressible spheres in an inviscid fluid,

Doinikov calculated the acoustic "pressure" (i.e., force) on rigid [47] and compressible spheres [48] by progressive and stationary sound waves of frequency f and acoustic energy flux I in a viscous fluid with a sound speed S. Remarkably, while King [45] showed that particles would migrate in the direction of the sound wave for an inviscid fluid, Doinikov calculated that fluid viscosity makes particles travel against the wave [47]. In the limit where $\pi f d/S \ll d[\pi f \rho_g/(2\mu)]^{1/2} \ll 1$, which applies to nanoparticle suspensions, Doinikov simplified his more general expressions for the ultrasonic force $\mathbf{F}_u$ on a sphere created by a progressive wave emanating from a transducer of outward normal $\mathbf{n}$,

$$\mathbf{F}_u = -\frac{11}{30}\pi^{5/2}\Big(\frac{\rho_s}{\rho_g}-1\Big)\frac{If^{3/2}d^4}{S^2(\mu/\rho_g)^{1/2}}\ \mathbf{n}. \quad (16)$$

In dilute suspensions, nanoparticles subject to Stokes, ultrasonic and thermophoretic forces then reach a terminal velocity

$$\mathbf{v}_t = \mathbf{v}_T + \mathbf{v}_u = \quad (17)$$
$$-\frac{\mu}{\rho_g}\beta\nabla\ln T - \frac{11}{90}\pi^{3/2}\Big(\frac{\rho_s}{\rho_g}-1\Big)\frac{If^{3/2}d^3\rho_g^{1/2}}{S^2\mu^{3/2}}\ \mathbf{n}\ .$$

Thus, positive thermophoresis can be thwarted by applying a progressive sound wave in a direction $\mathbf{n}$ against the temperature gradient ∇T. In principle, this can be achieved if the ultrasonic transducer coincides with the hot wall. Negative thermophoresis would requires the opposite arrangement.

3.3. Diffusion

In a uniform temperature gradient aligned with $\mathbf{n}$, the thermophoretic and ultrasonic forces act as a net effective settling force similar to gravity. In this case, the particle mass diffusion flux has three components. The first arises from Brownian motion with diffusivity $D_{\text{s-e}}$ given by Eq. (12). The second is induced by local fluctuations in solid volume fraction resulting from the net advection of particles driven at the settling velocity $\mathbf{v}_t$. A paradox with the diffusion of non-colloidal particles settling under gravity is that the resulting diffusivity D_ν should, in theory, diverge with the size of the vessel containing the sedimenting suspension [49–53], despite experimental evidence to the contrary [54,55]. Using Lattice-Boltzmann numerical simulations, Nguyen and Ladd [56] suggested that polydispersity can provide a mechanism for the screening of the long-range interactions that cause this divergence. On the other hand, Mucha and Brenner [57] suggested a resolution of the paradox by introducing a hydrodynamic settling diffusivity that depends on the local solid volume fraction, as well as its gradient,

$$D_\nu = L|\mathbf{v}_t|\ f_\nu[\nu; |L\nabla\nu|; L/d]\ , \quad (18)$$

where the function

$$f_\nu[\nu; |L\nabla\nu|; L/d] \equiv C \times \quad (19)$$
$$\begin{cases} \nu^{1/2}(2L/d)^{1/2} & \text{if } |\nabla\nu| \leqslant |\nabla\nu|_{\text{crit}} \\ B^{3/2}(\frac{d}{2L})^{2/5}\frac{\nu^{4/5}}{|L\nabla\nu|^{3/5}} & \text{otherwise .} \end{cases}$$

Mucha and Brenner [57] fitted $B \simeq 1/2$ and $C \simeq 1$ to numerical simulations and wrote

$$|\nabla\nu|_{\text{crit}} = B\frac{\nu^{1/2}}{L}\Big(\frac{d}{2L}\Big)^{3/2}. \quad (20)$$

Because these equations pertain to settling forces aligned with gravity, they may be valid for unidirectional thermophoretic and/or ultrasonic forces. In particular, they might apply to the channel bounded by two infinite, parallel, flat, possibly sonified thermal walls that we consider in this section. As we later show, for practical values of $\nabla T \neq \mathbf{0}$, the settling diffusivity in Eq. (18) can dominate its Brownian counterpart. Therefore we expect that, although D_ν was originally derived for non-colloidal spheres, it may be relevant to nanoparticle suspensions as well. Unlike its Stokes-Einstein counterpart in Eq. (13), it also contributes to the particle-phase conductivity given by Eq. (5). At practical values of ∇T, the resulting magnitude of K_s may no longer be negligible. However, as we shall see, such K_s is only significant for short times.

The third diffusivity D_u possibly arises from particle agitation induced by ultrasounds. We estimate its magnitude by analogy with Eqs. (8), (11) and (12),

$$D_u \sim \frac{1}{3}\tau_s < \mathbf{v}_u^2 > \ , \quad (21)$$

where

$$< \mathbf{v}_u^2 >^{1/2} = \left(\frac{\rho_g}{\rho_s}\right)\frac{3}{\pi}\sqrt{\frac{I\ S}{\rho_g d^2 f^2}}\ \mathcal{L}(\omega;\omega_v) \quad (22)$$

is the rms particle velocity fluctuation induced by a plane ultrasonic wave. In the first approximation, Doinikov [47] calculated

$$\mathcal{L}(\omega;\omega_v) = |j_1(\omega)+\alpha_1 h_1(\omega)+2\beta_1 h_1(\omega_v)|\ , \quad (23)$$

where $j_1(\omega) = (\sin\omega/\omega^2) - \cos\omega/\omega$ is the spherical Bessel function of the first kind and order 1, $h_1(\omega) = -(\omega + \imath)\exp(\imath\omega)/\omega^2$ is a spherical Hankel function of the first kind and order 1, $\alpha_1(\omega;\omega_v) \equiv -[\mu_1\mu_3 + 2(1-\rho_g/\rho_s)^2 j_1(\omega)h_1(\omega_v)]/\mu_4$, $\beta_1(\omega;\omega_v) \equiv (1-\rho_g/\rho_s)[\mu_1 h_1(\omega) - \mu_2 j_1(\omega)]/\mu_4$, $\mu_1 = (1-\rho_g/\rho_s)j_1(\omega) - \omega j_1'(\omega)$, $\mu_2 = (1-\rho_g/\rho_s)h_1(\omega) - \omega h_1'(\omega)$, $\mu_3 = (1-2\rho_g/\rho_s)h_1(\omega_v) + \omega_v h_1'(\omega_v)$, $\mu_4 = \mu_2\mu_3 + 2(1-\rho_g/\rho_s)^2 h_1(\omega)h_1(\omega_v)$, primes denote the first derivative, and, to a good approximation for most suspensions, $\omega \simeq \pi f d/S$ and $\omega_v \simeq \omega^{1/2}[d\ S\rho_g/(4\mu)]^{1/2}(1+\imath)$ with $\imath^2 = -1$.

Figure 1 compares the magnitudes of $D_{\text{s-e}}$, D_u and D_ν for typical homogeneous ($\nabla\nu = \mathbf{0}$) and isothermal ($\nabla T = \mathbf{0}$) suspensions in a small vessel (no thermophoresis). In that figure, the abscissa is the particle diameter made dimensionless with ultrasonic frequency and sound speed. The lowest ω for these curves corresponds to small nanoparticles. The largest represent relatively big microparticles. Because $D_u \ll D_\nu, \forall\omega$, we can ignore the direct contribution D_u of the ultrasonic fluctuation velocity to the overall diffusivity. A practical consequence is that it would be difficult to augment the solid-phase conductivity K_s in Eq. (5) by manipulating D_u using ultrasonic particle agitation. In other words, unlike the macroscopic grains of Parts I and II [1], nanoparticles cannot be agitated to raise K_s appreciably without inducing particle migration. Such migration can be driven by ultrasounds and/or thermophoresis. If the latter prevails ($I = 0$, $\nabla T \neq \mathbf{0}$), the early stages in which the suspension is still nearly homogeneous ($\nabla\nu \simeq \mathbf{0}$) across two walls with temperature difference ΔT can exhibit a thermophoretic settling diffusivity $D_\nu \sim (\mu/\rho_g)\beta C\nu^{1/2}(2L/d)(\Delta T/\bar{T}) \gg D_{\text{s-e}}$,

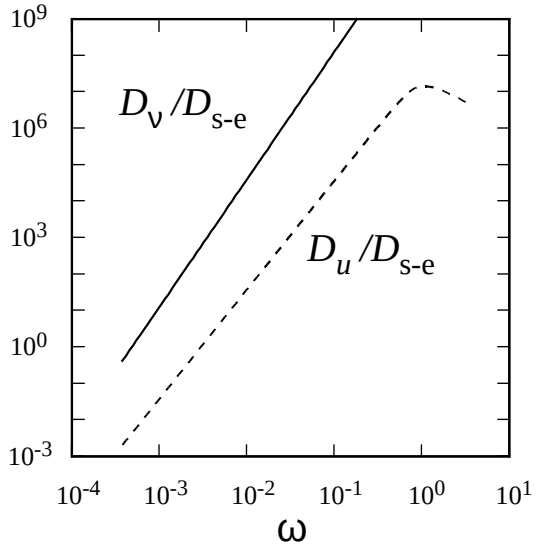

Figure 1. Diffusivity ratios $D_u/D_{\text{s-e}} = [\rho_g I S^2/(2\pi^2\rho_s f^3 k_b\bar{T}]\omega\mathcal{L}^2$ (dashed line) and $D_\nu/D_{\text{s-e}} = [11\sqrt{2}C/(30\pi)](\rho_s/\rho_g - 1)[(IS^{3/2}\rho_g^{1/2}L^{3/2})/(f^2\mu^{1/2}k_b\bar{T})]\nu^{1/2}\omega^{7/2}$ (solid line) vs. $\omega \simeq \pi f d/S$ for a homogeneous, isothermal suspension of, for example, copper nanoparticles in ethylene glycol ($S = 1660$ m/s) at $\nu = 0.01$ and $\bar{T} = 300$°K with ultrasonic forcing at a frequency $f = 20$ MHz and energy flux $I = 10^4$ W/m^2 in a channel with $L = 0.001$m. In this example, the lowest ω represents 10 nm particles.

which, as we shall see after analyzing particle migration, could result in significant, but ephemeral, values of K_s if thermophoresis is strong enough.

3.4. Governing equations

We now write the thermal governing equations and apply these to a channel between two parallel plates containing a suspension globally at rest. This derivation complements Buongiorno's, who treated the mixture as a single phase [19]. In contrast, because diffusion and advection of the dispersed particles both induce reverse fluxes in the liquid, we distinguish the mass balances of the dispersed and continuous phases separately. For the liquid, the balance is

$$\rho_g \frac{\partial(1-\nu)}{\partial t} + \rho_g \nabla\cdot[(1-\nu)\mathbf{u}] + \nabla\cdot\mathbf{j}_g'' = 0; \quad (24)$$

and for the solids,

$$\rho_s \frac{\partial \nu}{\partial t} + \rho_s \nabla\cdot[\nu\mathbf{v}] + \nabla\cdot\mathbf{j}_s'' = 0, \quad (25)$$

where $\mathbf{u}$ and $\mathbf{v}$ represent the mean velocities of liquid and solids, respectively. The total particle mass diffusion is

$$\mathbf{j}_s'' = -\rho_s D_s \nabla\nu \ , \quad (26)$$

where $D_s = D_{\text{s-e}} + D_\nu + D_u$. In a mixture at rest, such diffusion induces a reverse mass flux of liquid $\mathbf{j}_g''$. Because particles and liquid are incompressible, the two corresponding volume fluxes balance,

$$(\mathbf{j}_s''/\rho_s) + (\mathbf{j}_g''/\rho_g) = \mathbf{0}. \quad (27)$$

Adding Eqs. (24) and (25), and using Eq. (27), we find $\nabla\cdot[(1-\nu)\mathbf{u} + \nu\mathbf{v}] = 0$. Because neither phase can penetrate the walls, $\mathbf{u} = \mathbf{v} = \mathbf{0}$ there, and Eq. (27) integrates to

$$(1-\nu)\mathbf{u} + \nu\mathbf{v} = \mathbf{0}. \quad (28)$$

The balance of sensible energy of the liquid is

$$\rho_g \frac{\partial}{\partial t}[(1-\nu)h_g] + \rho_g \nabla\cdot[(1-\nu)h_g\mathbf{u}] \quad (29)$$
$$+\nabla\cdot(h_g\mathbf{j}_g'') + \nabla\cdot\mathbf{q}_g = 0 \ ;$$

and for the particles it is

$$\rho_s \frac{\partial}{\partial t}[\nu h_s] + \rho_s \nabla\cdot[\nu h_s\mathbf{v}] \quad (30)$$
$$+\nabla\cdot(h_s\mathbf{j}_s'') + \nabla\cdot\mathbf{q}_s = 0.$$

In these equations, h_g and h_s are the sensible enthalpies per unit mass of liquid and solid, respectively; $\mathbf{q}_g = -K_g\ \nabla T$ and $\mathbf{q}_s = -K_s\ \nabla T$ are the Fourier heat fluxes of the two phases sharing the common temperature T in the diffusion limit. Upon expanding the first two ∇-terms in Eqs. (29) and (30), simplifying the result using Eqs. (24) and (25), substituting the relation between $\mathbf{u}$ and $\mathbf{v}$ in Eq. (28), using $\partial h_g/\partial T \equiv c_g$ and $\partial h_s/\partial T \equiv c_s$, and adding the resulting equations for the solid and liquid phases, we find

$$\rho c \frac{\partial T}{\partial t} = (\rho_s c_s - \rho_g c_g)[-\nu\mathbf{v}\cdot\nabla T + D_s \nabla\nu\cdot\nabla T] \quad (31)$$
$$+\nabla\cdot[(K_g + K_s)\nabla T],$$

where

$$\rho c \equiv \rho_s c_s \nu + \rho_g c_g (1-\nu) \quad (32)$$

is the mixture specific heat per unit volume and $K_s = \nu\rho_s c_s D_s$ from Eq. (5).

Note that we ignored the term $D_s(\nabla\nu\cdot\nabla T)$ in Parts I and II [1]. In Part I, we did so because ν was assumed uniform. In Part II, although gravity produced a significant vertical gradient of volume fraction in the vibrated box, its direction was perpendicular to the horizontal temperature gradient, and thus $D_s(\nabla\nu\cdot\nabla T)$ likely vanished as well.

Our result in Eq. (31) differs from Buongiorno's [19] in the additional factor $(\rho_s c_s - \rho_g c_g)$, which arises from the reverse fluid flow induced by the mean solids velocity. It is interesting to note that this factor is positive for suspensions of iron ($\rho_s = 7870$ kg/m^3, $c_s = 447$ J/kg°K) and copper in ethylene glycol (EG), while it is negative for suspension of Al_2O_3 ($\rho_s = 3690$ kg/m^3, $c_s = 880$ J/kg°K) in water ($\rho_g = 1000$ kg/m^3, $c_g = 4179$ J/kg°K). Because Cu/EG and Fe/EG exhibited anomalously high apparent conductivities, and Al_2O_3 did not, Eq. (31) suggests at first glance that the anomaly could be related to some kind of particle flux, including thermophoresis.

However, as we shall calculate later, the term $\propto (\rho_s c_s - \rho_g c_g)$ in Eq. (31) is small relative to the conduction term involving $(K_g + K_s)$.

We now apply Eqs. (25) and (31) to a channel bound by two parallel thermal planes separated by the distance L and maintained at the respective temperatures $T^{\pm}$ at $y = \pm L/2$, where y is the coordinate perpendicular to the plates with origin at the center of the channel and pointing to the hot wall. As we shall later confirm, the Stokes relaxation time τ_s is several orders of magnitude smaller than hydrodynamic or heat transfer times scales. Therefore, in the mixture at rest, we equate the solid velocity to the terminal velocity of Eq. (17) for an isolated particle, suitably corrected for hindered settling at other than vanishing ν,

$$\mathbf{v} = \mathbf{v}_t / R_d. \tag{33}$$

We adopt the expression of Koch and Sangani [58], who determined $R_d(\nu)$ from numerical simulations. For $0 < \nu < 0.4$, they found

$$R_d = \frac{1 + 3(\nu/2)^{1/2} + (135/64)\nu \ln \nu + 17.14\nu}{1 + 0.681\nu - 8.48\nu^2 + 8.16\nu^3}; \tag{34}$$

for $\nu \geq 0.4$, they invoked Carman's empirical correlation [59]

$$R_d = \frac{10\nu}{(1-\nu)^3} + 0.7, \tag{35}$$

to which they added the constant 0.7 to match Eqs. (34) and (35) at $\nu = 0.4$.

Dimensionless variables and parameters are $y^\dagger \equiv y/L$, $T^\dagger \equiv (T - \bar{T})/\Delta T$ with $\bar{T} \equiv (T^+ + T^-)/2$ and $\Delta T \equiv (T^+ - T^-)$, $t^\dagger \equiv t(\bar{K}_g/\overline{\rho c})/L^2$, wall flux $q^\dagger \equiv qL/[\bar{K}_g \Delta T]$, conductivities $k^\dagger \equiv k/\bar{K}_g$ and diffusivities $D^\dagger \equiv D/(\bar{K}_g/\overline{\rho c})$, where the overbar denotes a quantity evaluated at the average solid volume fraction $\bar{\nu}$. The dimensionless governing equations are, for particle mass,

$$\frac{\partial \nu}{\partial t^\dagger} = \frac{\partial}{\partial y^\dagger}\Big[\frac{(\nu\ \beta\ \mathrm{Pr}/R_d)}{(T^\dagger + \bar{\theta})}\frac{\partial T^\dagger}{\partial y^\dagger}\Big] \tag{36}$$
$$+(\mathbf{e}_y \cdot \mathbf{n})\ \mathrm{Pe}_s \frac{\partial(\nu/R_d)}{\partial y^\dagger} + \frac{\partial}{\partial y^\dagger}\Big(D_s^\dagger \frac{\partial \nu}{\partial y^\dagger}\Big);$$

and for sensible energy,

$$[\nu + (1-\nu)C^\dagger]\frac{\partial T^\dagger}{\partial t^\dagger} = \tag{37}$$
$$(1 - C^\dagger)\Big\{\frac{(\beta\ \mathrm{Pr}\ \nu/R_d)}{(T^\dagger + \bar{\theta})}\Big(\frac{\partial T^\dagger}{\partial y^\dagger}\Big)^2 +$$
$$(\mathbf{e}_y \cdot \mathbf{n})\ (\nu/R_d)\ \mathrm{Pe}_s \frac{\partial T^\dagger}{\partial y^\dagger} + D_s^\dagger \frac{\partial \nu}{\partial y^\dagger}\frac{\partial T^\dagger}{\partial y^\dagger}\Big\} +$$
$$[\bar{\nu} + (1-\bar{\nu})C^\dagger]\frac{\partial}{\partial y^\dagger}\Big[(K_g^\dagger + K_s^\dagger)\frac{\partial T^\dagger}{\partial y^\dagger}\Big]\ ,$$

where, using Eqs. (5) and (32),

$$K_s^\dagger = \frac{\nu\ D_s^\dagger}{[\bar{\nu} + C^\dagger(1-\bar{\nu})]} \tag{38}$$

with $D_s^\dagger = \mathrm{Le}\ (1 + T^\dagger/\bar{\theta}) + D_\nu^\dagger + D_u^\dagger$. In this geometry, the dimensionless settling diffusivity is

$$D_\nu^\dagger = \Big|\frac{\beta\ \mathrm{Pr}}{(T^\dagger + \bar{\theta})}\frac{\partial T^\dagger}{\partial y^\dagger} + \mathrm{Pe}_s(\mathbf{e}_y \cdot \mathbf{n})\Big|\ f_\nu(\nu; \frac{\partial \nu}{\partial y^\dagger}; \frac{L}{d})\ . \tag{39}$$

As Fig. 1 showed, we can neglect the direct contribution of ultrasounds to the particle diffusivity

$$D_u^\dagger = \frac{\mathrm{Pr}}{6\pi^2}\Big(\frac{\rho_g^2\ I\ S}{\rho_s \mu^2\ f^2}\Big)\mathcal{L}^2, \tag{40}$$

which is always $\ll D_\nu^\dagger$, and ignore the dimensionless parameters therefrom. We also assume that the ultrasonic transducer normal $\mathbf{n}$ is either pointed along the unit vector $\mathbf{e}_y$ in the y-direction, or against it. Then for example, if $(\mathbf{e}_y \cdot \mathbf{n}) = -1$, the ultrasonic wave acts against the thermophoretic gradient when $T^+ > T^-$ and $\beta > 0$.

Nine dimensionless numbers arise from Eqs. (36)-(39). They are: the average solid volume fraction $\bar{\nu}$, the relative channel width L/d, the conductivity ratio ξ_s (or the slope $\partial(K_g/k_g)/\partial\nu$) specifying variations of the mixture conductivity with ν, the mixture Prandtl number $\mathrm{Pr} \equiv \mu/(\rho_g \bar{\alpha})$ with $\bar{\alpha} \equiv \bar{K}_g/\overline{\rho c}$, the ratio $C^\dagger \equiv (\rho_g c_g)/(\rho_s c_s)$ of specific heats per unit volume of the fluid and particle material, a Lewis number $\mathrm{Le} \equiv k_b \bar{T}/(3\pi\mu d\bar{\alpha})$ characterizing Brownian diffusion, the coefficient β in Eq. (15)

gauging the strength of thermophoresis, and the dimensionless ambient temperature $\bar{\theta} \equiv \bar{T}/\Delta T$; the dimensionless number characterizing ultrasonic forcing in the thermal problem is a Péclet number $\mathrm{Pe}_s \equiv |v_u|L/(\bar{K}_g/\overline{\rho c})$, where v_u is the ultrasonic terminal velocity in Eq. (17). For simplicity, we ignore sound attenuation in this problem. Thicker channels or dense suspensions could instead exhibit a diminishing local value of Pe_s [60]. In dimensionless form, the Stokes relaxation time $\tau_s^\dagger = (\rho_s/\rho_g)(d/L)^2/(18\mathrm{Pr})$ needed to reach the terminal velocity in Eq. (33) is $\ll 1$ for any practical condition involving nanoparticles.

Assuming $D_u^\dagger \ll D_\nu^\dagger$, we solve Eqs. (36) and (37) subject to an initial homogeneous suspension with linear temperature profile, $\nu = \bar{\nu}$ and $T^\dagger = y^\dagger$, and to the boundary conditions at $y^\dagger = \pm 1/2$

$$\left[\mathrm{Le}\left(1 + \frac{T^\dagger}{\bar{\theta}}\right) + D_\nu^\dagger\right]\frac{\partial \nu}{\partial y^\dagger} \quad (41)$$

$$+\frac{(\nu\ \beta\ \mathrm{Pr}/R_d)}{(\bar{\theta} + T^\dagger)}\frac{\partial T^\dagger}{\partial y^\dagger} + (\mathbf{e}_y \cdot \mathbf{n})\ \frac{\nu}{R_d}\ \mathrm{Pe}_s = 0\ ,$$

which reflect the absence of a particle flux through the walls, and $T^\dagger = \pm 1/2$ at $y^\dagger = \pm 1/2$, using MATLAB's pdepe routine. The latter automatically adjusts the time step for optimum stability. Because Eqs. (36) and (37) cannot guarantee that ν remains within the physical interval $0 \leqslant \nu < \nu_c$, where ν_c is the volume fraction of a randomly jammed packing [61], we occasionally (but rarely) enforce $\nu \in [0, \nu_c[$ in the following way: if at a point the numerical algorithm finds a value of $\nu < 0$, it substitutes $\nu = 0$ and $\partial\nu/\partial r^\dagger = 0$ in calculations involving that point. Similarly, if $\nu > \nu_c$, it enforces $\nu = \nu_c$ and $\partial\nu/\partial r^\dagger = 0$.

3.5. Thermophoretic migration

As Fig. 2 shows for conditions where settling diffusivity dominates its Brownian counterpart, positive thermophoresis causes small particles to congregate near the cold wall. Gharagozloo, et al [62] recently observed such migration using an infrared microscope with aluminum oxide nanoparticles suspended by deionized water in a parallel channel with $L = 500$ μm and $\bar{\theta} \simeq 8$. This migration makes the mixture conductivity inhomogeneous. Without ultrasonic forcing to

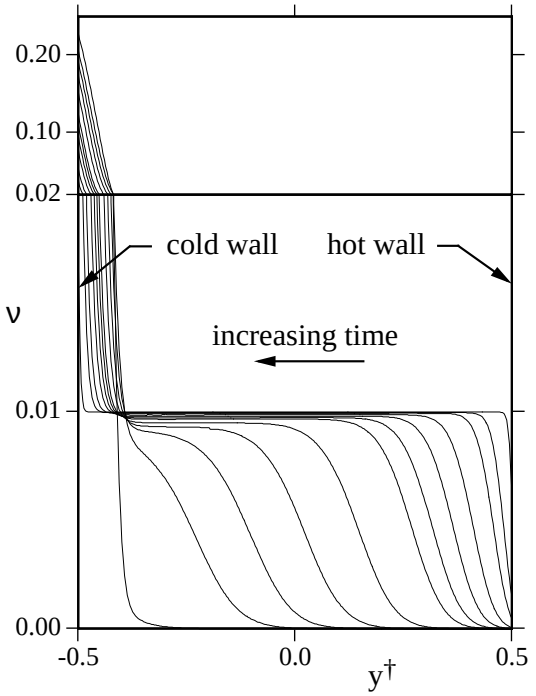

Figure 2. Profiles of solid volume fraction at increasing times for the conditions $\bar{\nu} = 0.01$, $\mathrm{Pr} = 146$, $\beta = 1.6\ 10^{-4}$, $\mathrm{Le} = 2.9\ 10^{-5}$, $\bar{\theta} = 7.5$, $\xi_s = 1600$, $C^\dagger = 0.78$, $L/d = 10^5$ and $\mathrm{Pe}_s = 0$ (no ultrasonic forcing), corresponding to 10 nm copper particles experiencing nominal, relatively weak positive thermophoresis with $\beta = 0.26k_g/(2k_g + k_s)$ and suspended by ethylene glycol in a channel 1 mm wide. From right to left, curves are plotted at successive times $t^\dagger = 1, 10, 20, 40, 60, 80, 100, 150, 200, 250, 300$ and 400. For $t^\dagger \gtrsim 400$, most particles congregate near the cold wall. For these conditions, a unit interval in $t^\dagger$ corresponds to 10.4 s. To obtain these curves, we discretized the channel thickness in 320 uniform intervals. Note the change of scale to illustrate accumulation at $y^\dagger = -1/2$.

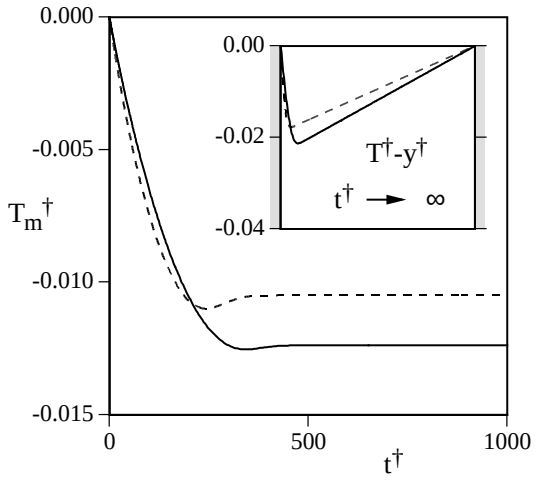

Figure 3. Dimensionless mixed-mean temperature $T_m^\dagger$ vs. dimensionless time for conditions of Fig. 2 (no ultrasounds, $\beta > 0$). The inset shows the difference $T^\dagger - y^\dagger$ between the actual temperature and a linear temperature profile from hot wall (right) to cold wall (left) when the mixed-mean temperature has reached a steady value ($t^\dagger \to \infty$) or, equivalently, when both wall heat fluxes have returned to balance. Because $|T^\dagger - y^\dagger| \lesssim 0.02$, it is reasonable to assume $\partial T^\dagger/\partial y^\dagger \simeq 1$. Solid lines show the solution of Eqs. (36)-(37) with $D_s^\dagger = \mathrm{Le}\ (1 + T^\dagger/\bar{\theta}) + D_\nu^\dagger$. The dashed lines illustrate the role of the settling diffusivity D_ν by making it vanish.

counteract thermophoresis, K_g gradually drifts toward the clear fluid conductivity at the hot wall, while increasing at the cold wall. To assess consequences of this imbalance in mixture conductivity, we write the global unsteady energy balance in the channel,

$$\frac{d}{dt}\int_{y=-L/2}^{+L/2}[\rho_s\nu h_s + \rho_g(1-\nu)h_g]dy = -q^+ + q^-, \tag{42}$$

where $q^\pm < 0$ are wall heat fluxes at $y = \pm L/2$. We then define the mixed-mean temperature

$$T_m - \bar{T} \equiv \int_{y=-L/2}^{+L/2}[\rho_s c_s\nu + \rho_g c_g(1-\nu)](T-\bar{T})dy \Big/ \int_{y=-L/2}^{+L/2}[\rho_s c_s\nu + \rho_g c_g(1-\nu)]dy. \tag{43}$$

Assuming that specific heats vary little across the channel, we write $h_{s,g} \simeq \bar{h}_{s,g} + c_{s,g}(T - \bar{T})$, substitute in Eq. (42), and write the result in dimensionless form

$$\frac{dT_m^\dagger}{dt^\dagger} \simeq -q^{\dagger +} + q^{\dagger -}. \tag{44}$$

Thus, the rate of change of $T_m^\dagger$ represents the net gain (or loss) of sensible energy in the channel. Figure 3 plots the time-history of $T_m^\dagger$ for conditions of Fig. 2. Starting from a homogeneous suspension with zero mean dimensionless temperature, particle migration causes a greater escape of energy at the cold wall than the corresponding input at the hot wall, $0 < -q^+ < -q^-$, thus reducing $T_m^\dagger$. Eventually, particles reside mostly near the cold wall ($t^\dagger > 400$), $T_m^\dagger$ is invariant, and thermal fluxes at both walls return to balance. At this steady state, the temperature profile is everywhere beneath the linear profile imposed initially in the homogeneous suspension (inset, Fig. 3). Such imbalances of mass and temperature arise faster with greater values of β, which are typically exhibited by solids of relatively low conductivity.

Because, as the inset of Fig 3 shows, $\partial T^\dagger/\partial y^\dagger \simeq +1$, and because $|T^\dagger| \lesssim 1/2 \ll \bar{\theta}$, thermophoresis is set by the group $\beta \mathrm{Pr}/\bar{\theta}$ that appears in

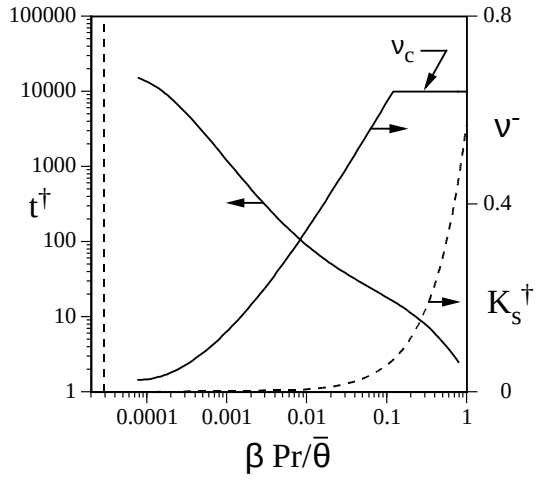

Figure 4. Left axis: dimensionless time for $|T_m^\dagger|$ to reach 99% of its steady, long-term value; right axis: long-time solid volume fraction at the cold wall ($y^\dagger = -1/2$, $t \to \infty$) and "flash" particle-phase conductivity $K_s^\dagger \equiv K_s/\bar{K}_g$ vs. $\beta \mathrm{Pr}/\bar{\theta}$. (An example of $T_m^\dagger$ vs. time appears in Fig. 3). Calculations were carried out by varying $\bar{\theta}$ at fixed $\mathrm{Pr} = 146$ and for $\beta = 1.6\ 10^{-4}, 3.3\ 10^{-4}, 6.5\ 10^{-4}$ and $1.3\ 10^{-3}$ without ultrasonic forcing, $\mathrm{Pe}_s = 0$. Values of $\bar{\nu}$, Le, ξ_s, $C^\dagger$, and L/d, see Fig. 2. The vertical dashed line marks $\beta \mathrm{Pr}/\bar{\theta} = \mathrm{Le}$, to the right of which settling diffusivity increasingly dominates its Brownian counterpart.

Eqs. (36), (37), (39) and (41). In particular, it is stronger when the mean temperature gradient is high or, equivalently, when $\bar{\theta}$ is low. The left axis of Fig. 4 shows how much time is needed to reach a steady $T_m^\dagger$ for several values of $\bar{\theta}$. (Other quantities reach a steady-state in roughly the same time). The right axis shows the corresponding maximum value of the solid volume fraction ν^-, which, in the absence of ultrasonic forcing and $\beta > 0$, occurs at the cold wall. In the absence of ultrasounds, the relative strength of the settling and Brownian diffusivities is

$$\frac{D_\nu}{D_{\text{s-e}}} = \frac{|\beta|\mathrm{Pr}/\bar{\theta}}{\mathrm{Le}(1+T^\dagger/\bar{\theta})^2}\, f_\nu \left|\frac{\partial T^\dagger}{\partial y^\dagger}\right| \simeq \frac{|\beta|\mathrm{Pr}/\bar{\theta}}{\mathrm{Le}}\, f_\nu\,, \tag{45}$$

which is governed by the ratio $(|\beta|\mathrm{Pr}/\bar{\theta})/\mathrm{Le}$. As Fig. 4 shows, for low temperature gradients or weak thermophoresis with $\mathrm{Le} \sim \beta \mathrm{Pr}/\bar{\theta}$ and $\beta > 0$, Brownian diffusion counteracts the inexorable settling of particles near the cold wall, and the steady value of ν^- at the cold wall satisfies $\bar{\nu} \lesssim \nu^- < \nu_c$. In contrast, if $\mathrm{Le} \ll \beta \mathrm{Pr}/\bar{\theta}$, Brownian diffusion is negligible and particles drift to the cold wall with $\nu^- \to \nu_c$. During this process, the settling diffusion produces a particle-phase conductivity, which is calculated by substituting D_ν in Eq. (5), and is showed as a dashed line measured on the right axis of Fig. 4. For conditions of Fig. 2 at the nominal thermophoretic coefficient $\beta = 1.6\ 10^{-4}$, this conductivity is small, $K_s^\dagger = K_s/\bar{K}_g \simeq 2\ 10^{-3}$, so settling diffusion adds little to K_g. If however, as Giddings, et al suggested [34], metal nanoparticles effectively possess a much higher $\beta \simeq 3.5\ 10^{-2}$ commensurate with silica particles, then $K_s^\dagger \simeq 0.4$, thus constituting a significant enhancement over $K_g^\dagger = K_g/\bar{K}_g \simeq 1$.

However, this enhanced settling conductivity, which occurs shortly after the thermal temperature gradient is imposed, does not persist long throughout the channel, as positive thermophoresis quickly sweeps solids away from the hot wall. For this reason, we call this "flash" conductivity. To illustrate its ephemeral existence, we calculate the dimensionless average channel conductivity by integrating contributions of elementary

slices of width $dy^\dagger$ to the overall thermal resistance of the channel,

$$\bar{K}^\dagger \equiv \Big[\int_{y^\dagger=-1/2}^{+1/2} \frac{\bar{K}_g}{K_g + K_s} dy^\dagger \Big]^{-1} . \qquad (46)$$

We find that $\bar{K}^\dagger$ returns to $\bar{K}_g$ on a time scale much shorter than the time to steady-state plotted in Fig. 4. For example, with parameters of Fig. 2 and $\beta = 0.035$, the relaxation time of $\bar{K}^\dagger$ is $t^\dagger \sim 6\ 10^{-7}$; for $\beta = 0.017$, it is $\sim 9\ 10^{-7}$. (However, note that these times scales are still much greater than the Stokes relaxation time $\tau_s^\dagger = 3\ 10^{-13}$). Therefore, while possible, this "flash" enhancement of the particle-phase conductivity is quickly followed by strong inhomogeneities, it requires a strong temperature gradient, it is ephemeral, and it only exists for particles of small material conductivities or anomalously high thermophoretic coefficient. Similar flash conductivity would also arise with negative thermophoresis.

3.6. Ultrasonic mitigation

Our analysis suggests that ultrasounds can frustrate thermophoretic particle migration, which is captured by the first term on the right side of Eq. (36). Because $\partial T^\dagger/\partial y^\dagger \simeq 1$ and $|T^\dagger| \ll \bar{\theta}$, and because particle diffusion vanishes at uniform ν, the right side of Eq. (36) is nearly balanced or, equivalently, ν becomes invariant when ultrasounds are applied such that $(\mathbf{e}_y \cdot \mathbf{n}) = -1$ for $\beta > 0$ (or $+1$ for $\beta < 0$) and

$$\mathrm{Pe}_s = \frac{|\beta|\ \mathrm{Pr}}{\bar{\theta}}. \qquad (47)$$

Figure 5 plots the dimensionless time needed for the disappearance of 99% of the initial volume fraction at any wall. If no ultrasounds are applied ($\mathrm{Pe}_s = 0$), this takes $t^\dagger \simeq 38$ for the relatively modest thermopheretic coefficient $\beta = 1.6\ 10^{-4}$ to wipe particles off the hot wall at $\bar{\theta} = 7.5$. When the ultrasonic terminal velocity is raised, this depletion time increases, as particle migration gets thwarted by the ultrasonic force. The time diverges to ∞ as Pe_s approaches the value prescribed in Eq. (47). When that value is exceeded, ultrasounds drive particles in the opposite direction, the cold wall is now depleted, and the time to do so decreases with increasing Pe_s.

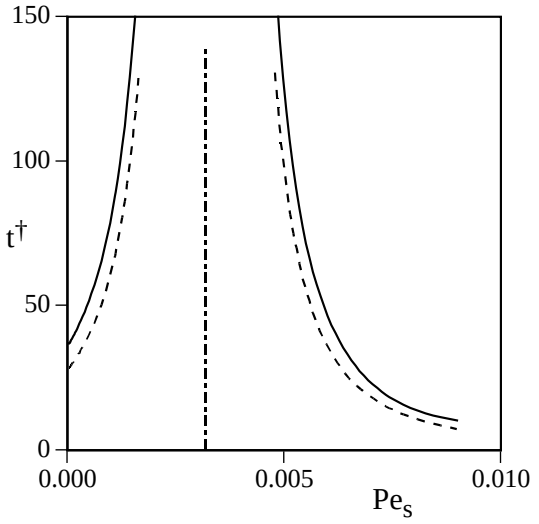

Figure 5. Dimensionless time to deplete the volume fraction at a wall down to 1% of its original value vs. Péclet number for the conditions of Fig. 2, $(\mathbf{e}_y \cdot \mathbf{n}) = -1$ and $\beta > 0$. The vertical dashed line marks the value of $\mathrm{Pe}_s \sim 0.0032$ in Eq. (47). To its left, thermophoresis is stronger than ultrasonic forcing, and solids migrate away from the hot wall. To its right, ultrasounds are stronger, and solids leave the cold wall.

Unfortunately, conventional transducers might not be strong enough to mitigate the thermophoretic migration of very small particles. To achieve the Péclet number prescribed by Eq. (47), one must supply the acoustic energy flux

$$I = \frac{90}{11\pi^{3/2}} \frac{|\beta|\ S^2 \mu^{5/2}}{f^{3/2}\ d^3\ \rho_g^{3/2} L\ \bar{\theta}} , \qquad (48)$$

which rises steeply as d decreases. For example, 10nm copper particles in ethylene glycol at 300°K with $\beta = 1.6\ 10^{-4}$ in a channel 1 mm wide require $I = 11$ MW/m^2 at $f = 20$MHz to oppose $\Delta T = 1$°K, which is clearly impossible. Commercial transducers producing $\lesssim 10$kW/m^2 at 20MHz can only reach Pe_s in Eq. (47) with

$d \gtrsim 100$nm.

For conditions typical of Fig. 2, the three terms in curly brackets on the right side of Eq. (37) are much less important to the balance of energy than the conduction term featuring $(K_g^\dagger + K_s^\dagger)$. Therefore, the role of thermophoresis is largely captured by Eq. (36), which predicts the local evolution of ν and the corresponding variations of $(K_g^\dagger + K_s^\dagger)$.

Figures 3 and 5 also illustrate the role of settling diffusion with dashed lines representing the solutions of Eqs. (36)-(37) without $D_\nu^\dagger$. As these figures show, settling diffusion merely delays thermophoretic migration and the subsequent return to a thermal steady-state.

In summary, suspensions of small particles in the diffusion limit differ from their macroscopic counterpart by the existence of a thermopheric coupling between temperature gradient and solid volume fraction, which can create severe concentration inhomogeneities by moving solids toward cold ($\beta > 0$) or hot ($\beta < 0$) regions. In principle, ultrasonic forcing can counteract this effect by fitting a transducer on a hot wall. However, the required sonic energy flux for nanoparticles generally exceeds the performance of available ultrasonic systems. In channels with unidirectional ∇T, thermophoresis acts as a settling force similar to gravity. If it is strong enough, it can result in a significant enhancement of the self-diffusive particle-phase conductivity, which suspensions at $\nabla T = \nabla \nu = \mathbf{0}$ do not achieve with Brownian self-diffusion alone, but such enhancement is ephemeral.

Because thermophoresis drives time-varying suspension inhomogeneities, we examine in the next section whether conventional techniques like hot-wire conductimetry, which are meant for homogeneous fluids of invariant properties, provide a reliable measurement.

4. Hot-wire conductimetry

The conductivity measurement technique employed with most nanoparticle suspensions is the transient hot-wire method, suitably adapted to handle electrically-conductive liquids [63]. A constant volumetric heat flow rate is produced by the Joule effect in a thin cylindrical wire by switching on a constant electrical current suddenly at time zero, while a known length of wire is immersed in a fluid initially at the temperature T_∞. Because conductance of the wire material is a linear function of temperature, the overall resistance of the wire, which is recorded with a bridge, is a measure of its average temperature

$$\bar{T}_w = \frac{1}{\pi r_w^2} \int_{r=0}^{r_w} T_w \; 2\pi r dr, \tag{49}$$

where r is the radial coordinate from the wire's centerline and r_w is the radius of the electrically conductive wire core. Hot wire data is commonly reduced by calculating the apparent conductivity

$$k_a \equiv \frac{\dot{q}}{4\pi} \Big/ \frac{d\bar{T}_w}{d \ln t}, \tag{50}$$

in which $\dot{q}$ is the heat supplied to a unit of wire length [6]. If this measurement is carried out long enough after electricity is first switched on, k_a tends asymptotically to the invariant conductivity of the homogeneous medium in which the wire is immersed. Nonetheless, it would be imprudent to wait too long, since the rising temperature could promote free convection that may augment the apparent rate at which the wire loses heat [29].

In this problem, it is natural to introduce new dimensionless variables, which, for convenience, we will denote with the same † superscript used earlier. Thus in this section, we make time dimensionless with the wire radius and the mixture thermal diffusivity at the mean solid volume fraction, $t^\dagger \equiv \bar{\alpha} t / r_w^2$; radii dimensionless with wire radius, $r^\dagger \equiv r/r_w$; thermal conductivities and diffusivities with their mixture counterparts, $k^\dagger \equiv k/\bar{K}_g$, $\alpha^\dagger \equiv \alpha/\bar{\alpha}$; and temperature with the mixture conductivity and the electrical heat rate supplied per unit wire length, $T^\dagger \equiv (T - T_\infty)\; 2\pi \bar{K}_g / \dot{q}$.

4.1. Role of insulating sheath

Carslaw and Jaeger [64] provided analytical expressions for a wire of infinite conductivity, possibly protected by a sheath, and immersed in a homogeneous medium. Without a sheath, the solution of Carslaw and Jaeger yields the apparent

conductivity

$$k_a^\dagger = \frac{\pi^2}{8\Pi^2 t^\dagger} \Big/ \int_{\iota=0}^{\infty} \frac{\exp(-t^\dagger \iota^2)}{\iota[(\iota J_0 - \Pi J_1)^2 + (\iota Y_0 - \Pi Y_1)^2]}, \tag{51}$$

where $J_0(\iota)$ and $J_1(\iota)$ are Bessel functions of the first kind, $Y_0(\iota)$ and $Y_1(\iota)$ are Bessel functions of the second kind, and $\Pi \equiv 2(\overline{\rho c})/(\rho_w c_w)$ is twice the ratio of the specific heats per unit volume of the mixture and that of the wire.

Nagasaka and Nagashima [63] derived expressions for a wire of finite conductivity with a sheath for $t^\dagger \gtrsim o(1)$ after the onset of electrical heating. Substituting their results in Eq. (50), we find

$$\frac{1}{k_a^\dagger} = 1 + \frac{1}{2t^\dagger}\Big\{ \frac{k_p^\dagger}{\alpha_p^\dagger} - \frac{k_w^\dagger}{\alpha_w^\dagger} + \frac{r_p^{\dagger 2}}{\alpha_p^\dagger}(1-k_p^\dagger) - \frac{1}{\alpha_p^\dagger} + \frac{1}{2\alpha_w^\dagger} - \Big(\frac{1-k_p^\dagger}{4k_w^\dagger}\Big)\Big(\frac{1}{\alpha_w^\dagger} - \frac{1}{\alpha_p^\dagger}\Big) - 2\Big(\frac{1}{\alpha_p^\dagger} - \frac{k_w^\dagger}{\alpha_w^\dagger k_p^\dagger}\Big)\ln(r_p^\dagger)\Big\} - \frac{1}{2t^\dagger}\Big\{ \frac{k_p^\dagger}{\alpha_p^\dagger} - \frac{k_w^\dagger}{\alpha_w^\dagger} + \Big(1 - \frac{k_p^\dagger}{\alpha_p^\dagger}\Big) r_p^{\dagger 2}\Big\} \ln\Big(\frac{4t^\dagger}{\exp(\gamma) r_p^{\dagger 2}}\Big), \tag{52}$$

where $\gamma \simeq 0.577$ is Euler's constant. In this equation, the subscripts p and w denote material properties of the sheath and the conductive wire core, respectively; and the outer radius of the sheath is r_p.

As Nagasaka and Nagashima [63] noted, the presence of a sheath, which is necessary to handle electrically conductive solids [6], delays reaching the asymptote $k_a^\dagger \to 1$, paradoxically more so if the sheath is made of a highly thermally conductive electrical insulator (Fig. 6). Clearly, it is important to wait a sufficient time $t^\dagger \gtrsim 1000$ to reach the asymptote, and to report this time along with thermal conductivity data. For the system shown in Fig. 6, this represents about 4 s. Alternately, as Knibbe and Raal showed [65], it is possible to exploit the time-history of $\bar{T}_w^\dagger$ at smaller times to extract the fluid thermal conductivity and diffusivity simultaneously.

During long measurements, small particles can be subject to thermophoresis, which draws them

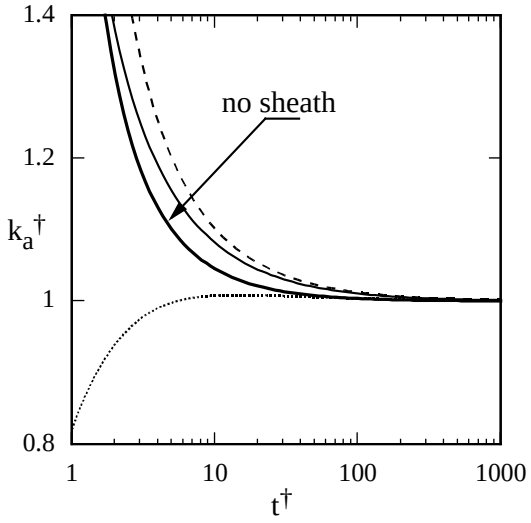

Figure 6. Instantaneous ratio of the thermal conductivity inferred by the hot-wire method and the actual fluid conductivity vs. dimensionless time for typical hot wire systems. The heavy solid line labeled "no sheath" denotes a platinum wire core of 20μm diameter with properties $\rho_w = 21450$ kg/m^3, $c_w = 133$ J/kg°K and $k_w = 72$ W/m°K immersed in ethylene glycol. The thin solid line is the same fluid, but the core has a protective sheath of 7.5μm thickness with $\rho_p = 1350$ kg/m^3, $c_p = 1280$ J/kg°K and $k_p = 0.28$ W/m°K. The rising dotted line represent the same combination, but with a sheath of lower conductivity $k_p = 0.1$ W/m°K, while the falling dashed line is for a more conductive sheath with $k_p = 0.5$ W/m°K.

away from the wire if $\beta > 0$. If the wire was immersed in the suspension long enough to cause particles to adhere to its surface, positive thermophoresis might also resuspend these particles. Conversely, if $\beta < 0$, the suspension might progressively densify at the wire, particularly if the applied electrical power is large. We discuss next to what extent these phenomena should be taken into consideration.

4.2. Thermophoretic migration and resuspension

Ignoring ultrasonic forcing ($\mathbf{v}_s = \mathbf{0}$), as well as effects of radiation, particle aggregation and electrophoresis, we substitute the thermophoretic velocity in Eq. (33) for $\mathbf{v}$ and write Eqs. (25) and (31) in the radial coordinate,

$$\frac{\partial \nu}{\partial t} = \frac{1}{r}\frac{\partial}{\partial r}\Big(r\frac{\nu\beta}{R_d}\frac{\mu}{\rho_g}\frac{\partial \ln T}{\partial r}\Big)+\frac{1}{r}\frac{\partial}{\partial r}\Big(rD_s\frac{\partial \nu}{\partial r}\Big) \quad (53)$$

and

$$\rho c\frac{\partial T}{\partial t} = (\rho_s c_s - \rho_g c_g)\Big\{\frac{\nu\beta}{R_d}\frac{\mu}{\rho_g}\frac{1}{T}\Big(\frac{\partial T}{\partial r}\Big)^2 \quad (54)$$
$$+D_s\frac{\partial \nu}{\partial r}\frac{\partial T}{\partial r}\Big\}+\frac{1}{r}\frac{\partial}{\partial r}\Big[r(K_g+K_s)\frac{\partial T}{\partial r}\Big],$$

where $D_s = D_\nu + D_{\text{s-e}}$.

Far away from the wire ($r \to \infty$), the fluid is at rest with $\mathbf{u} = \mathbf{v} = \mathbf{0}$, $\nu = \bar{\nu}$, $T = T_\infty$, and Eq. (28) remains valid. For the boundary condition at $r = r_w$, we write the balance of mass and energy fluxes at the wire surface projected along its normal $\mathbf{e}_r$. For the mass,

$$\mathbf{J}'' \cdot \mathbf{e}_r = (\rho_s \nu \mathbf{v} + \mathbf{j}_s'') \cdot \mathbf{e}_r, \quad (55)$$

where $\mathbf{J}'' = J''\mathbf{e}_r$ is a possible resuspension mass flux of particles previously adhered to the wire, which we only consider if $\beta > 0$, and

$$\mathbf{q} = h_s[\rho_s\nu\mathbf{v} + \mathbf{j}_s''] \cdot \mathbf{e}_r \quad (56)$$
$$+h_g[\rho_g(1-\nu)\mathbf{u} + \mathbf{j}_g''] \cdot \mathbf{e}_r + (\mathbf{q}_s + \mathbf{q}_g) \cdot \mathbf{e}_r,$$

where $\mathbf{q} = \dot{q}/(2\pi r_w)\mathbf{e}_r$ is the radial electrical energy flux supplied by the wire to the suspension. Using Eqs. (27), (28) and (55), and the definitions of c_s and c_g, the energy boundary condition becomes

$$\mathbf{q} = -(K_g+K_s)\nabla T+\frac{\mathbf{J}''}{\rho_s}\int_0^T(\rho_s c_s-\rho_g c_g)dT, \quad (57)$$

where, for compatibility with the expression for thermophoretic velocity, the reference temperature of enthalpies is taken to be absolute zero. It is interesting to note that, in the absence of a resuspension flux, such reference temperature need not be invoked, as the term containing the temperature integral in Eq. (57) would vanish. In that event, thermophoresis would not affect the form of the Fourier energy boundary condition either. For simplicity, we assume that $(\rho_s c_s - \rho_g c_g)$ is invariant with temperature to carry out the integral.

To estimate the magnitude of the resuspension flux with $\beta > 0$, we assume that it is driven by the difference $\mathbf{F} = 3\pi\mu d(\mathbf{v}_T - \mathbf{v})$ between the thermophoretic and Stokes forces working against the attractive van der Waals force $\mathbf{F}_v = -[A_{132}\ d/(12\eta^2)]\mathbf{e}_r$ acting on particles previously adhered to the wire surface. In this expression, A_{132} is the Hamaker constant of particle of index 1 adhered to the wire of index 2 in the liquid of index 3, and η is the gap between wire and particle [66]. We write that the energy per unit time needed to liberate adhered particles from a unit surface of the wire is supplied by the net force $\mathbf{F}$ as it detaches particles and accelerates them from rest to the thermophoretic terminal velocity,

$$\frac{J''}{m}\int_{\eta=\eta_0}^{\infty} A_{132}\frac{d}{12\eta^2}d\eta = N\int_{v=0}^{v_T} F dv, \quad (58)$$

where N is the surface number density of adhered particles and η_0 is the initial adhesion gap. Carrying out the integrals,

$$J'' = 3\pi^2\rho_s d^3 N\mu\ v_T^2\ \eta_0/A_{132}. \quad (59)$$

If no particle returns to adhere again to the wire, the supply of adhered particles decreases with time according to $dN/dt = -J''/m$, where $N \propto J''$ from Eq. (59). Assuming for simplicity that v_T changes slower than N, the surface number density decreases as

$$N = N_0\exp(-t/\tau), \quad (60)$$

where $\tau = A_{132}/(18\pi\mu v_T^2\eta_0)$. For particles initially adhered in n_ℓ layers at a surface fraction ν_s, $N_0 = 4n_\ell\nu_s/(\pi d^2)$.

Adopting the reference time, radius, temperature, conductivities and diffusivities introduced earlier in this section, we write Eqs. (53) and (54) in dimensionless form. For mass conservation,

$$\frac{\partial\nu}{\partial t^\dagger}=\frac{1}{r^\dagger}\frac{\partial}{\partial r^\dagger}\Big[\frac{r^\dagger(\nu\beta\ \mathrm{Pr}/R_d)}{(T^\dagger+\theta_\infty)}\frac{\partial T^\dagger}{\partial r^\dagger}\Big] \quad (61)$$
$$+\frac{1}{r^\dagger}\frac{\partial}{\partial r^\dagger}\Big\{r^\dagger\Big[\mathrm{Le}_\infty\Big(1+\frac{T^\dagger}{\theta_\infty}\Big)+D_\nu^\dagger\Big]\frac{\partial\nu}{\partial r^\dagger}\Big\},$$

and for energy,

$$[\nu+C^\dagger(1-\nu)]\frac{\partial T^\dagger}{\partial t^\dagger}= \quad (62)$$
$$(1-C^\dagger)\Big\{\frac{(\nu\beta\ \mathrm{Pr}/R_d)}{(T^\dagger+\theta_\infty)}\Big(\frac{\partial T^\dagger}{\partial r^\dagger}\Big)^2+$$
$$\Big[\mathrm{Le}_\infty\Big(1+\frac{T^\dagger}{\theta_\infty}\Big)+D_\nu^\dagger\Big]\Big(\frac{\partial\nu}{\partial r^\dagger}\Big)\Big(\frac{\partial T^\dagger}{\partial r^\dagger}\Big)\Big\}+$$
$$\frac{[\bar\nu+C^\dagger(1-\bar\nu)]}{r^\dagger}\frac{\partial}{\partial r^\dagger}\Big[r^\dagger(K_g^\dagger+K_s^\dagger)\frac{\partial T^\dagger}{\partial r^\dagger}\Big],$$

subject to the initial conditions $\nu=\bar\nu$ and $T^\dagger=0$ for $t^\dagger<0$ and to the boundary conditions $\nu=\bar\nu$ and $T^\dagger=0$ as $r^\dagger\to\infty$. Substituting J'' from Eq. (59), the boundary condition (55) for particle mass at $r^\dagger=1$ becomes

$$\Big[\mathrm{Le}_\infty\Big(1+\frac{T^\dagger}{\theta_\infty}\Big)+D_\nu^\dagger\Big]\Big(\frac{\partial\nu}{\partial r^\dagger}\Big) \quad (63)$$
$$+\frac{(\mathrm{Pr}\ \nu\beta/R_d)}{(\theta_\infty+T^\dagger)}\Big(\frac{\partial T^\dagger}{\partial r^\dagger}\Big)=$$
$$12\pi\frac{\mathrm{Pr}\ \beta^2\ \Gamma_r}{(\theta_\infty+T^\dagger)^2}\exp(-t^\dagger/\tau^\dagger)\Big(\frac{\partial T^\dagger}{\partial r^\dagger}\Big)^2\mathrm{sign}\Big(\frac{\partial T^\dagger}{\partial r^\dagger}\Big),$$

and its counterpart for mixture energy is

$$(K_g^\dagger+K_s^\dagger)\frac{\partial T^\dagger}{\partial r^\dagger} \quad (64)$$
$$+12\pi\frac{(1-C^\dagger)}{[\bar\nu+C^\dagger(1-\bar\nu)]}\frac{\mathrm{Pr}\ \beta^2\ \Gamma_r}{(\theta_\infty+T^\dagger)}\times$$
$$\exp(-t^\dagger/\tau^\dagger)\Big(\frac{\partial T^\dagger}{\partial r^\dagger}\Big)^2\mathrm{sign}\Big(\frac{\partial T^\dagger}{\partial r^\dagger}\Big)=-1,$$

in which the direction of thermophoretic resuspension is specified by the sign of $\partial T^\dagger/\partial r^\dagger$, and $\tau^\dagger\equiv\tau\bar\alpha/r_w^2$ is the dimensionless characteristic time for resuspension of adhered particles. For $\beta<0$, we set $J''=0$ or, equivalently, we ignore the terms $\propto\Gamma_r$ in Eqs. (63) and (64).

We calculate $K_s\dagger$ in Eqs. (62) and (64) using Eq. (38). However, unlike the parallel geometry in section 3, thermophoresis around the wire is no longer unidirectional. Thus it is unclear whether the settling diffusion D_ν described by Eq. (18) remains valid in the presence of the central gradient ∇T directed toward the wire axis. It is equally unclear which length scale should be substituted for L in that equation. A crude assumption is to ignore the central character of the thermophoretic force, to adopt Eq. (18), and to equate L to the size of the container. In this case,

$$D_\nu^\dagger=\frac{C\ |\beta|\ \mathrm{Pr}}{(T^\dagger+\theta_\infty)}\Big|\frac{\partial T^\dagger}{\partial r^\dagger}\Big|\times \quad (65)$$
$$\begin{cases}\nu^{1/2}(\frac{2r_w}{d})^{1/2}(\frac{L}{r_w})^{3/2} & \text{if } |\frac{\partial\nu}{\partial r^\dagger}|\leqslant|\frac{\partial\nu}{\partial r^\dagger}|_{\rm crit}\\ B^{3/2}(\frac{d}{2r_w})^{2/5}\frac{\nu^{4/5}}{|\frac{\partial\nu}{\partial r^\dagger}|^{3/5}} & \text{otherwise,}\end{cases}$$

where

$$\Big|\frac{\partial\nu}{\partial r^\dagger}\Big|_{\rm crit}=\Big(\frac{d}{2r_w}\Big)^{3/2}\frac{B\nu^{1/2}}{(L/r_w)^{5/2}}. \quad (66)$$

As we shall see, this settling diffusivity has marginal effects on hot-wire conductimetry, and thus it is not crucial to know its precise form for the central force field of interest.

Nine dimensionless numbers arise from Eqs. (61) to (66). They are: $\bar\nu$, ξ_s (or $\partial(K_g/k_g)/\partial\nu$), Pr, $C^\dagger$, a new Lewis number $\mathrm{Le}_\infty\equiv k_bT_\infty/(3\pi\mu d\bar\alpha)$, β, the dimensionless ambient temperature $\theta_\infty\equiv 2\pi\bar K_gT_\infty/\dot q$, the relative vessel size L/r_w and, if thermophoresis-driven resuspension occurs with $\beta>0$, $\Gamma_r\equiv n_\ell\nu_s d\ \mu^2\eta_0/(r_w\rho_gA_{132})$. Thus, more particles will resuspend if Γ_r is large or, equivalently, if the Hamaker constant is weak or if many particles have adhered to the wire. Although Γ_r increases also with d, we expect the thermophoretic driving force to become negligible once inertia becomes important, in which case Eqs. (61) to (64) no longer apply.

We solve the governing equations using MATLAB's pdepe routine in the domain $r^\dagger\in[1,R^\dagger]$ and over the period $t^\dagger\in[0,t_f^\dagger]$. We choose the outer limit $R^\dagger$ of the radial domain such that the residual temperature at $R^\dagger$ is much smaller than at the wire surface, and that no particle

moving at the thermophoretic velocity can ever reach $R^\dagger$. Because $\partial T^\dagger/\partial r^\dagger \simeq -1$ at $r^\dagger = 1$, these conditions imply $R^\dagger \gg 1 + T_w^\dagger(t_f^\dagger)$ and $R^\dagger \gg |\beta|$ Pr $t_f^\dagger/\theta_\infty$. We run numerical calculations at successively smaller radial increments until further refinements become inconsequential. Because the pdepe routine cannot handle terms $\propto (\partial T^\dagger/\partial r^\dagger)^2$ in boundary conditions (63) and (64), we iterate successive solutions in which the magnitude of these terms are calculated from the previous iteration. We use Carslaw and Jaeger's analytical solution for the first iteration, and we stop when the root-mean-square difference between the temperature time-histories at $r^\dagger = 1$ from two consecutive iterations is $< 10^{-5}$. Convergence typically requires no more than five iterations. We enforce $\nu \in [0, \nu_c[$ as outlined in section 3. From the solution, we calculate the apparent conductivity using the dimensionless form of Eq. (50),

$$\frac{1}{k_a^\dagger} = 2\frac{dT^\dagger}{d\ln t^\dagger}\Big|_{r^\dagger=1}. \tag{67}$$

Figures 7 and 8 illustrate the results. As Buongiorno [19] noted, the terms proportional to $(\partial T^\dagger/\partial r^\dagger)^2$ and $(\partial\nu/\partial r^\dagger)(\partial T^\dagger/\partial r^\dagger)$ in Eq. (62) are negligible compared with the last conduction term in the equation. To gauge how thermophoresis affects the particle population in the wire's vicinity, we compute the relative excess or deficit of particle mass $M^\dagger$ in the region $1 \leqslant r^\dagger \leqslant 2$,

$$M^\dagger = \int_{r^\dagger=1}^{2} (\nu - \bar\nu)\, 2\pi r^\dagger dr^\dagger \Big/ \int_{r^\dagger=1}^{2} \bar\nu\, 2\pi r^\dagger dr^\dagger, \tag{68}$$

and plot it versus time in Fig. 7. A deficit of particle has $M^\dagger < 0$; the value $M^\dagger = -1$ represents clear fluid; an excess has $M^\dagger > 0$. Note that settling diffusion has a modest effect on $M^\dagger$, just delaying the migration of particles away from the wire (dotted lines, Fig. 7). Moreover, unlike its role in augmenting $K_s^\dagger$ for a short time in the parallel channel of section 3, "flash" settling diffusion has no discernable influence on the time-history of $k_a^\dagger$ from the hot wire, except perhaps at $t^\dagger < 10^{-2}$, which has no practical importance to this measurement.

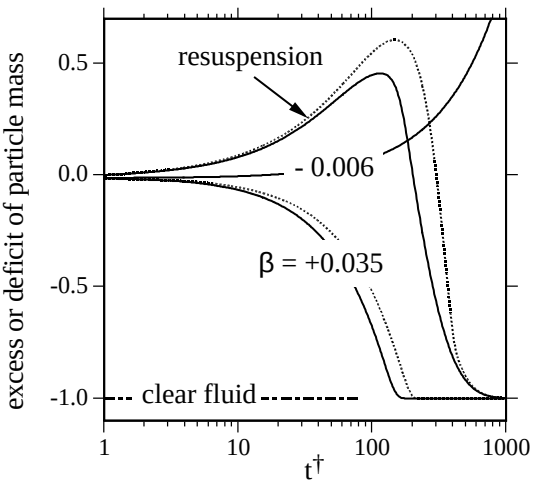

Figure 7. Excess ($M^\dagger > 0$) or deficit ($-1 \leqslant M^\dagger < 0$) of particle mass in the region $1 \leqslant r^\dagger \leqslant 2$ vs. dimensionless time for the conditions $\bar\nu = 0.01$, $\partial(K_g/k_g)/\partial\nu = 3$, Pr $= 146$, $C^\dagger = 0.78$, $\mathrm{Le}_\infty = 3\ 10^{-5}$, and $\theta_\infty = 490$, corresponding to 10nm particles of copper in ethylene glycol at 300°K probed by a wire of 20 μm diameter at $\dot q = 1$W/m. For such conditions, a unit interval in $t^\dagger$ corresponds to 4.2 ms. To obtain these curves, we discretized space in 3200 intervals in the range $1 \leqslant r^\dagger \leqslant 100$. Solid lines represent solutions of Eqs. (61)-(64) without settling diffusion, $D_\nu = 0$. Dotted lines are obtained with $D_\nu^\dagger$ from Eq. (65) with $L/r_w = 50$. The bottom two curves are obtained with relatively strong positive thermophoresis, $\beta = 0.035$, for which the particles behave like silica ($k_s = 1.4$W/m°K) [34], and no prior particle adhesion, $n_\ell\nu_s = 0$. The curve labeled "resuspension" represens thermophoresis-driven resuspension with $\beta = 0.035$ and $\Gamma_r = 9.4$, corresponding to $A_{132} = 20\ 10^{-20}$J, $\eta_0 = 0.17$nm [66], and a 1 μm layer of initially adhered particles, $n_\ell\nu_s = 100$. The rising curve is for negative thermophoresis with $\beta = -0.006$. (D_ν has negligible effects in this case).

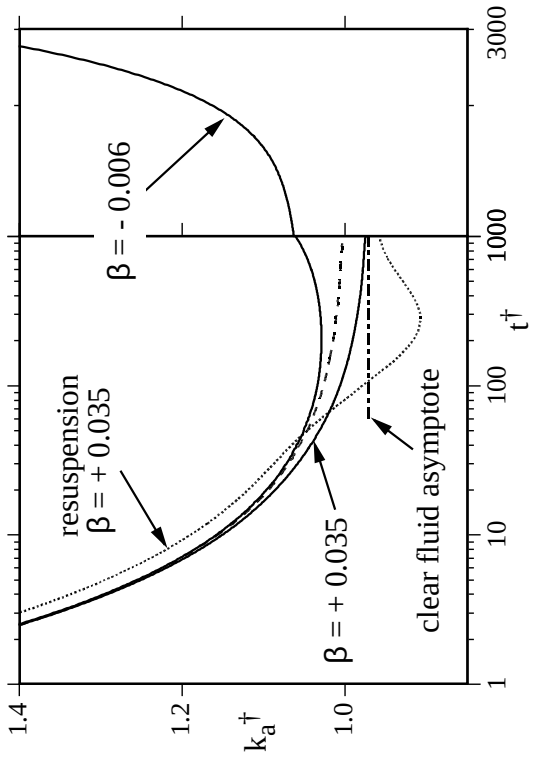

Figure 8. Dimensionless apparent conductivity $k_a/\bar{K}_g$ inferred from hot-wire measurements with Eq. (50) vs. dimensionless time for conditions of Fig. 7. The dashed line has $\beta = 0$ (no thermophoresis) and, like its counterparts in Fig. 6, asymptotes to $k_a^\dagger \to 1$ as $t^\dagger \to \infty$. The bottom solid line has $\beta = +0.035$ and $\Gamma_r = 0$ (no resuspension), and the dotted line has $\beta = +0.035$ and $\Gamma_r = 9.4$. Because of thermophoretic migration of particles away from the hot wire, the dotted and dashed curves asymptote to the clear fluid value $k_a^\dagger \to k_g/\bar{K}_g < 1$ marked by the horizontal line labeled "clear fluid". The top solid line has negative thermophoresis with $\beta = -0.006$. The magnification of time scale on the right shows how rapidly such negative thermophoresis can accumulate particles near the wire and raise the apparent conductivity.

Figures 7 and 8 distinguish two regimes of thermophoretic migration depending on the sign of β. For nominal properties of copper nanoparticles in ethylene glycol ($\beta = 0.26k_g/(k_s + 2k_g) \simeq 1.6\ 10^{-4}$), positive thermophoresis causes negligible migration of solids away from the wire, unless the measurement is carried out too long, $t^\dagger \gg 1000$. If instead copper exhibited effective thermophoretic coefficients as high as those suggested by Giddings, et al [34], $\beta \simeq 0.035$, then substantial deficits of solids could quickly appear next to the wire. However, as Fig. 8 shows, such deficit would lead to apparent conductivities k_a that are *lower*, instead of higher, than that of the base fluid, as $k_a^\dagger \to k_g/\bar{K}_g < 1$ as $t^\dagger \to \infty$.

Relatively strong particle resuspension could produce a temporary excess of solids near the wire, resulting in values of $k_a^\dagger$ larger than without thermophoresis at comparable times $t^\dagger < 40$. In spite of this, resuspension should eventually exhaust the initial supply of adhered particles (Eq. 60, $t^\dagger \gtrsim 200$). At that stage, the apparent conductivity k_a would dip below k_g, and finally return to the clear fluid asymptote as thermophoresis draws particles away from the wire. Therefore, even if an exceptional number of particles had previously fouled the wire, particle resuspension should only play a minor role in the transient measurement. In general, if Eastman, et al [6] waited long enough to record apparent conductivity, *positive* thermophoresis cannot explain the anomalous increase in $k_{\rm eff}$ that they reported.

In contrast, *negative* thermophoresis has a more profound effect on the apparent conductivity. As Figs. 7 and 8 show, the relatively modest $\beta = -0.006$ can cause a densification of the mixture near the wire, thus leading to a late upsurge of $k_a^\dagger$. However, because thermophoretic diffusivity typically grows with T [39,41], and because temperature gradually rises in hot-wire conductimetry, β may not remain negative at long times. On the other hand, because the temperature at which β becomes > 0 appears to increase with ν [40], β might remain < 0 despite the growth of T near the wire. If it does, then negative thermophoresis could be responsible for a substantial, albeit artificial, augmentation of the apparent conductivity at long times. A similar artifact

at long times may also arise from the onset of free convection around the wire [29].

However, if hot-wire conductimetry properly accounted for the role of the sheath in delaying approach to the asymptote (Fig. 6), and if thermophoresis remained positive, explanations for the thermal anomalies of metal nanoparticles must be found elsewhere. Keblinski, et al [7] dismissed the role of ballistic phonons and Xue, et al [16] that of liquid layering. Ben-Abdallah [17] dismissed near-field interactions. Prasher, et al [10] pointed out that the interfacial resistance at the particle surface [67] should decrease $k_{\rm eff}$. Our analysis of the diffusion limit in section 2.2 agreed with others [7,8,10,19] that Brownian diffusion of thermal energy is also negligible. On the other hand, Vadasz, et al [18] suggested that enhancements may be due to hyperbolic conduction. Leong, et al [14] proposed that the ordered interfacial layer of liquid molecules at the solid surface could have much higher conductivity than the base fluid, thus raising the effective volume fraction of highly conductive material in the mixture.

Particle aggregation also plays an important role in nanofluids. Lin, et al [68–70] described the fractal nature of colloid aggregates and identified the universality of diffusion-limited and reaction-limited regimes of aggregation. Prasher, et al [13] showed that nanoparticles could form such fractal clusters occupying the fraction ν_a of the suspension volume and exhibiting high effective cluster conductivity $k_{\rm cl}$. In fact, Hong, et al [11] observed clusters on the order of ~ 1 μm, which they could not dissolve completely by ultrasounds. For percolating metal clusters with $\xi_s \ggg 1$, it is plausible that connected particle chains would produce $k_{\rm cl}/k_g \gg 1$, despite the clusters' relatively dilute internal volume fraction $\nu_{\rm cl}$ and the presence of interfacial Kapitza resistance at particle contact regions [14,16]. With overall volume fraction $\nu = \nu_a\nu_{\rm cl}$, the mixture conductivity would then become $K_g/k_g \simeq 1 + 3\nu_a = 1 + 3\nu/\nu_{\rm cl}$. Thus, the presence of clusters with high intrinsic $k_{\rm cl}$ could effectively rescale volume fraction and raise the slope of $\partial(K_g/k_g)/\partial\nu$ from 3 to $3/\nu_{\rm cl}$.

It is unclear how thermophoretic forces would affect such fractal clusters. However, the data of Putnam and Cahill [36,39] and Vigolo, et al [43] suggest that β is independent of particle diameter. Because the viscous settling of a cluster is typically set by its outer size, the thermophoretic migration might be described by substituting that size wherever d appears in the dimensionless numbers of section 3.4.

5. Conclusions

We have examined the role of particle agitation in enhancing the effective conductivity of fluid-solid suspensions. In Part I, we showed that, because macroscopic grains rarely exchange significant heat during their ephemeral collisions with each other and with walls, the enhancement is a competition between two rate-limiting processes, namely the ability of particles to self-diffuse and to exchange heat with the surrounding fluid [1]. Accordingly, we distinguished two regimes, called the "diffusion" and "exchange" limits, in which one or the other process dominates. In Part II, we tested the theory in the exchange limit by vigorously vibrating spheres in a box traversed by a controlled thermal heat flux, and obtained a heat flux enhancement as high as a factor of 20.

In Part III, we illustrated the diffusion limit by considering the transfer of heat through dilute suspensions of small colloidal spheres in an incompressible liquid. In this regime, which is governed by diffusion, particles exchange, on average, negligible heat with their surroundings, thus locally adopting the thermal temperature of the fluid. They also exhibit Brownian agitation, which could in principle enhance the thermal conductivity of the solid phase. However, unlike massive grains having a self-diffusive conductivity weakly dependent on particle concentration, the particle conductivity associated with Brownian self-diffusion is proportional to solid volume fraction, thus making the resulting enhancement too small to matter. Unlike the macroscopic grains considered in Part II, the Brownian motion of nanoparticles is not sufficient to agitate the surrounding fluid and augment its effective conductivity either [28].

On the other hand, for small particles, the existence of macroscopic temperature gradients in-

duces a thermophoretic migration of solids [32], which prevents the mixture from achieving a steady homogeneous concentration. In cases where the temperature gradient is uniform, the thermophoretic force causes a hindered settling resembling sedimentation and similarly provoking an additional diffusion [57], the magnitude of which can exceed its Brownian counterpart. Through volume conservation, the thermophoretic advection and settling diffusion cause reverse fluxes in the fluid, even in a suspension globally at rest. Therefore, although the fluid-solid mixture possesses a single thermal temperature, one should distinguish the thermal governing equations of the two phases, which exhibit different advection velocities and diffusion fluxes.

As Putnam, et al showed [37,39], thermophoresis can drive particles to regions that are cold ($\beta > 0$) or hot ($\beta < 0$), depending on solvent composition, temperature, and volume fraction [40]. If thermophoresis is intense, for example with particles having relatively low material conductivity, or with metal particles with anomalous surface potential distribution [34], the thermophoretic settling diffusion can induce a particle-phase "flash" conductivity augmenting significantly the mixture conductivity captured by homogenization models [22]. However, this enhancement is ephemeral, as thermophoresis inevitably creates inhomogeneities in particle concentration.

Our calculations suggested a technique to oppose particle thermophoretic migration by placing an ultrasonic transducer emitting progressive acoustic waves from a hot wall [47]. Unfortunately, such ultrasonic relief of thermophetic migration is only conceivable for solids larger than typical nanoparticles. We also estimated that the self-diffusion associated with ultrasonic particle fluctuation velocity is small compared with the settling diffusivity driven by ultrasonic particle advection.

We also considered how the gradual migration of nanoparticles away from hot surfaces affects the reliability of transient hot-wire conductimetry, which is meant for homogeneous fluids of invariant properties. We recalled that an electrically-insulating sheath causes a delay in the time needed for the apparent thermal conductivity to reach its asymptote [63], thus implying that wire measurements with conductive nanoparticles be carried out at long times, but not too long for free convection to play a role [29], and not with excessive electrical power that positive thermophoresis may deplete (or negative thermophoresis augment) the particle population at the wire. In this context, because time scales as wire radius squared, we recommend that hot-wire conductimetry data be reported together with measurement time delay, electrical power, wire geometry [71], and solvent composition [37].

We showed that, as positive thermophoresis depletes the particle population near the wire, it should reduce the long-time asymptotic value of the apparent conductivity. Thus, the anomalous increase in the long-term hot-wire conductivity of metal nanoparticles [6] cannot be attributed to positive thermophoresis, unless measurements were carried out too soon. We also examined whether the resuspension of particles previously adhered to the wire played any role. While such resuspension by positive thermophoresis could create a temporary increase in apparent conductivity, the gradual departure of particles from the wire and its vicinity should again result in a smaller apparent long-term conductivity, thus making it unlikely, once again, for positive thermophoresis to be responsible for anomalous hot-wire conductivity measurements.

However, we showed that negative thermophoresis, which can occur, for example, in aqueous suspensions of charged polystyrene spheres at relatively low ionic strength or temperature [37], could let the apparent hot-wire conductivity rise at long times due to particle migration toward the wire. Finally, we recalled the conclusions of others [68–70] that nanoparticle clustering likely plays an important role in the transport properties of nanofluids, including thermal conductivity.

6. Acknowledgements

The authors are grateful to Philippe Ben-Abdallah, Jean-Louis Barrat, Simon Biggs, Jacopo Buongiorno, Stephen Choi, Jacob

Eapen, David Erickson, William Evans, Patricia Gharagozloo, Pawel Keblinski, Brian Kirby, Donald Koch, Cécile Reynaud, Jonathan Selinger, David Venerus, Rolf Verberg and David Weitz for helpful information. They are indebted to Shawn Putnam for sharing an advance copy of her thesis, and to David Cahill for illuminating discussions on negative thermophoresis.

REFERENCES

1. X. Chen, M. Louge. Heat transfer enhancement in suspensions of agitated solids - Part I: Theory - Part II: Experiments in the exchange limit. *Int. J. Heat Mass Transfer* (2007), in press.
2. X. -Q. Wang, A. S. Mujumdar. Heat transfer characteristics of nanofluids: a review. *Int. J. Thermal Sciences* **46** (2007) 1-19.
3. J. A. Eastman, S. R. Phillpot, S. U. S. Choi, P. Keblinski. Thermal transport in nanofluids. *Annu. Rev. Mater. Res.* **34** (2004) 219-246.
4. J. C. Maxwell. *Electricity and Magnetism*, Clarendon Press, Oxford, UK (1873).
5. P. Keblinski, J. A. Eastman, D. G. Cahill. Nanofluids for thermal transport. *Materials Today* (June 2005) 36-44.
6. J. A. Eastman, S. U. S. Choi, S. Li, W. Yu, L. J. Thompson. Anomalously increased effective thermal conductivities of ethylene glycol-based nanofluids containing copper nanoparticles. *Appl. Phys. Lett.* **78** (2001) 718-720.
7. P. Keblinski, S. R. Phillpot, S. U. S. Choi, J. A. Eastman. Mechanisms of heat flow in suspensions of nano-sized particles (nanofluids). *Int. J. Heat Mass Transfer* **45** (2002) 855-863.
8. W. Evans, J. Fish, P. Keblinski. Role of Brownian motion hydrodynamics on nanofluid thermal conductivity. *Applied Phys. Lett.* **88** (2006) 093116.
9. S. P. Jang, S. U. S. Choi. Role of Brownian motion in the enhanced thermal conductivity of nanofluids. *Applied Phys. Lett.* **84** (2004) 4316-4318.
10. R. Prasher, P. Bhattacharya, P. E. Phelan. Thermal conductivity of nanoscale colloidal solutions (nanofluids). *Phys. Rev. Lett.* **94** (2005) 025901.
11. K. S. Hong, T. -K. Hong, H. -S. Yang. Thermal conductivity of Fe nanofluids depending on the cluster size of nanoparticles. *App. Phys. Lett.* **88** (2006) 031901.
12. T. -K. Hong, H. -S. Yang. Nanoparticle-dispersion-dependent thermal conductivity in nanofluids. *J. Korean Phys. Soc.* **47** (2005) S321-S324.
13. R. Prasher, W. Evans, P. Meakin, J. Fish, P. Phelan, P. Keblinski. Effect of aggregation on thermal conduction in colloidal nanofluids. *Applied Phys. Lett.* **89** (2006) 143119.
14. K. C. Leong, C. Yang, S. M. S. Murshed. A model for the thermal conductivity of nanofluids - the effect of interfacial layer. *J. Nanoparticle Res.* **8** (2006) 245-254.
15. M. Vladkov, J. -L. Barrat. Modeling transient absorption and thermal conductivity in a simple nanofluid. *Nano Lett.* **6** (2006) 1224-1228.
16. L. Xue, P. Keblinski, S. R. Phillpot, S. U. S. Choi, J. A. Eastman. Effect of liquid layering at the liquid-solid interface on thermal transport. *Int. J. Heat Mass Transfer* **47** (2004) 4277-4284.
17. P. Ben-Abdallah. Heat transfer through near-field interactions in nanofluids. *Appl. Phys. Lett.* **89** (2006) 113117.
18. J. J. Vadasz, S. Govender, P. Vadasz. Heat transfer enhancement in nano-fluids suspensions: possible mechanism and explanations. *Int. J. Heat Mass Transfer* **48** (2005) 2673-2683.
19. J. Buongiorno. Convective transport in nanofluids. *J. Heat Transfer* **128** (2006) 240-250.
20. S. A. Putnam, D. G. Cahill, P. V. Braun, Z. Ge, R. G. Shimmin. Thermal conductivity of nanoparticle suspension. *J. Appl. Phys.* **99** (2006) 084308.
21. D. C. Venerus, M. S. Kabadi, S. Lee, V. Perez-Luna. Study of thermal transport in nanoparticle suspensions using forced Rayleigh scattering. *J. Appl. Phys.* **100** (2006) 094310.

22. R. T. Bonnecaze, J. F. Brady. The effective conductivity of random suspensions of spherical particles. *Proc. Roy. Soc. Lond. A* **432** (1991) 445-465.
23. N. F. Carnahan, K. E. Starling. Equation of state for non-attracting rigid spheres. *J. Chem. Phys.* **51** (1969) 635-636.
24. M. Y. Louge, J. Mohd.-Yusof, J. T. Jenkins. Heat transfer in the pneumatic transport of massive particles. *Int. J. Heat Mass Transfer* **36** (1993) 265-275.
25. W. G. Vincenti, C. K. Kruger. Introduction to Physical Gas Dynamics. Krieger, NY (1965).
26. R. J. Hunter. Foundations of Colloidal Science, second edition. Oxford University Press, NY (2001).
27. E. G. D. Cohen, I. M. de Schepper. Comments on "Scaling of transient hydrodynamic interactions in concentrated suspensions". *Phys. Rev. Lett.* **75** (1995) 2252.
28. J. Eapen, W. C. Williams, J. Buongiorno, L.-W. Hu, S. Yip. Mean-field versus microconvection effects in nanofluid thermal conduction. *Phys. Rev. Lett.* **99** (2007) 095901.
29. R. Rusconi, W. C. Williams, J. Buongiorno, R. Piazza, L.-W. Hu. Numerical analysis of convective instabilities in a transient short-hot-wire setup for measurement of liquid thermal conductivity. *Int. J. Thermophysics* **28** (2007) 1131-1146.
30. M. Groschl. Ultrasonic separation of suspended particles. Part I: Fundamentals. *Acustica* **84** (1998) 432-447.
31. A. Haake, A. Neild, D. -H. Kim, J. -E. Ihm, Y. Sun, J. Dual, B. -K. Ju. Manipulation of cells using an ultrasonic pressure field. *Ultrasound in Med. & Biol.* **31** (2005) 857-864.
32. G. S. McNab, A. Meisen. Thermophoresis in liquids. *J. Colloid Interface Sci.* **44** (1973) 339-346.
33. P. S. Epstein. Zür Theorie des Radiometers. *Z. Physik* **54** (1929) 537-563.
34. J. C. Giddings, P. M. Shinudu, S. N. Semenov. Thermophoresis of metal particles in a liquid. *J. Colloid Interface Sci.* **176** (1995) 454-458.
35. S. A. Putnam, D. G. Cahill. Micron-scale apparatus for measurements of thermodiffusion in liquids. *Rev. Sci. Instrum.* **75** (2004) 2368-2372.
36. S. A. Putnam. Thermal probes of nanoparticle interfaces: Thermodiffusion and thermal conductivity of nanoparticle suspensions. *Ph.D. thesis*, University of Illinois at Urbana-Champaign (2007).
37. S. A. Putnam, D. G. Cahill. Transport of nanoscale Latex spheres in a temperature gradient. *Langmuir* **21** (2005) 5317-5323.
38. A. Würger. Heat capacity-driven inverse Soret effect of colloidal nanoparticles. *Europhys. Lett.* **74** (2006) 658-664.
39. S. A. Putnam, D. G. Cahill, G. C. L. Wong. Temperature dependence of thermodiffusion in aqueous suspensions of charged nanoparticles. *Langmuir* **23** (2007) 9221-9228.
40. H. Ning, J. Buitenhuis, J. K. G. Dhont, S. Wiegand. Thermal diffusion behavior of hard-sphere suspensions. *J. Chem. Phys.* **125** (2006) 204911.
41. S. Iacopini, R. Rusconi, R. Piazza. The "macromolecular tourist": Universal temperature dependence of thermal diffusion in aqueous colloidal suspensions. *Eur. Phys. J. E* **19** (2006) 59-67.
42. E. Bringuier. On the notion of thermophoretic velocity. *Phil. Mag.* **87** (2007) 873-883.
43. D. Vigolo, G. Brambilla, R. Piazza. Thermophoresis of microemulsion droplets: Size dependence of the Soret effect. *Phys. Rev. E* **75** (2007) 040401(R) .
44. J. Happel, H. Brenner. Low Reynolds number hydrodynamics. Prentice-Hall, NY (1965).
45. L. V. King. On the acoustic radiation pressure on spheres. *Proc. R. Soc. Lond. A* **147** (1934) 212-240.
46. K. Yosioka, Y. Kawasima. Acoustic radiation pressure on a compressible sphere. *Acustica* **5** (1955) 167-173.
47. A. A. Doinikov. Acoustic radiation pressure on a rigid sphere in a viscous liquid. *Proc. R. Soc. Lond. A* **447** (1994) 447-466.
48. A. A. Doinikov. Acoustic radiation pressure on a compressible sphere in a viscous liquid. *J. Fluid Mech.* **267** (1994) 1-21.

49. G. J. Kynch. A theory of sedimentation. *Trans. Faraday Soc.* **48** (1952) 166-176.
50. G. K. Batchelor. Sedimentation in a dilute dispersion of spheres. *J. Fluid Mech.* **52** (1972) 245-268.
51. R. E. Caflisch, J. H. C. Luke. Variance in the sedimentation speed of a suspension. *Phys. Fluids* **28** (1985) 759-760.
52. R. H. Davis, A. Acrivos. Sedimentation of non-colloidal particles at low Reynolds numbers. *Ann. Rev. Fluid Mech.* **17** (1985) 91-118.
53. D. L. Koch. Hydrodynamic diffusion in a suspension of sedimenting point particles with periodic boundary conditions. *Phys. Fluids* **6** (1994) 2894-2900.
54. H. Nicolai, E. Guazzelli. Effects of the vessel size on the hydrodynamic diffusion of sedimenting spheres. *Phys. Fluids* **7** (1995) 3-4.
55. H. Nicolai, B. Herzhaft, E. J. Hinch, L. Oger, E. Guazzelli. Particle velocity fluctuations and hydrodynamic self-diffusion of sedimenting non-Brownian spheres. *Phys. Fluids* **7** (1995) 12-23.
56. N. -Q. Nguyen, A. J. C. Ladd. Sedimentation of hard-sphere suspensions at low Reynolds number. *J. Fluid Mech.* **525** (2005) 73-104.
57. P. J. Mucha, M. P. Brenner. Diffusivities and front propagation in sedimentation. *Phys. Fluids* **15** (2003) 1305-1313.
58. D. L. Koch, A. S. Sangani. Particle pressure and marginal stability limits for a homogeneous monodisperse gas fluidized bed: kinetic theory and numerical simulations. *J. Fluid Mech.* **400** (1999) 229-263.
59. P. C. Carman. The determination of the specific surface area of powder *J. Soc. Chem. Ind.* **57** (1937) 225-236.
60. P. D. M. Spelt, M. A. Norato, A. S. Sangani, M. S. Greenwood, L. L. Tavlarides. Attenuation of sound in concentrated suspensions: theory and experiments. *J. Fluid Mech.* **430** (2001) 51-86.
61. S. Torquato. Nearest-neighbor statistics for packings of hard spheres and disks. *Phys. Rev. E* **51** (1995) 3170-3182.
62. P. E. Gharagozloo, K. E. Goodson, J. K. Eaton. Impact of thermodiffusion on temperature fields in stationary nanofluids. *Proceedings of IPACK 2007*, ASME InterPACK'07, July 8-12, Vancouver, BC, IPACK2007-33293, American Society of Mechanical Engineers (2007), pp. 1-6.
63. Y. Nagasaka, A. Nagashima. Absolute measurement of the thermal conductivity of electrically conducting liquids by the transient hot-wire method. *J. Phys. E: Sci. Instrum.* **14** (1981) 1435-1440.
64. H. S. Carslaw, J. C. Jaeger. Conduction of heat in solids, second edition. Oxford at the Clarendon Press (1959), p. 341-347.
65. P. G. Knibbe, J. D. Raal. Simultaneous measurements of the thermal conductivity and thermal diffusivity of liquids. *Int. J. of Thermophysics* **8** (1987) 181-191.
66. J. N. Israelachvili. Intermolecular and surface forces, second edition. Academic Press, San Diego, CA (1991).
67. O. M. Wilson, X. Hu, D. G. Cahill, P. V. Braun. Colloidal metal particles as probes of nanoscale thermal transport in fluids. *Phys. Rev. B* **66** (2002) 224301.
68. M. Y. Lin, H. M. Lindsay, D. A. Weitz, R. C. Ball, R. Klein, P. Meakin. Universality in colloid aggregation. *Nature* **339** (1989) 360-362.
69. M. Y. Lin, H. M. Lindsay, D. A. Weitz, R. C. Ball, R. Klein, P. Meakin. Universality of fractal aggregates as probed by light scattering. *Proc. R. Soc. Lond. A* **423** (1989) 71-87.
70. M. Y. Lin, H. M. Lindsay, D. A. Weitz, R. Klein, R. C. Ball, P. Meakin. Universal diffusion-limited colloid aggregation. *J. Phys.: Condens. Matter* **2** (1990) 3093-3113.
71. R. A. Perkins, M. L. V. Ramirez, C. A. Nieto de Castro. Thermal conductivity of saturated liquid toluene by use of anodized tantalum hot wires at high temperatures. *J. Res. Natl. Inst. Stand. Technol.* **105** (2000) 255-265.